

NASA/TM-2007-214881  
ARL-TR-3883



# Analysis of the Effects of Sea Disposal on a One-Ton Container

*Wade C. Jackson*  
*U.S. Army Research Laboratory*  
*Vehicle Technology Directorate*  
*NASA Langley Research Center, Hampton, Virginia*

*Karen E. Jackson and Edwin L. Fasanella*  
*NASA Langley Research Center, Hampton, Virginia*

*John Kelley*  
*U.S. Army Research Laboratory*  
*Weapons and Materials Research Directorate*  
*Aberdeen Proving Ground, Maryland*

## The NASA STI Program Office . . . in Profile

Since its founding, NASA has been dedicated to the advancement of aeronautics and space science. The NASA Scientific and Technical Information (STI) Program Office plays a key part in helping NASA maintain this important role.

The NASA STI Program Office is operated by Langley Research Center, the lead center for NASA's scientific and technical information. The NASA STI Program Office provides access to the NASA STI Database, the largest collection of aeronautical and space science STI in the world. The Program Office is also NASA's institutional mechanism for disseminating the results of its research and development activities. These results are published by NASA in the NASA STI Report Series, which includes the following report types:

- **TECHNICAL PUBLICATION.** Reports of completed research or a major significant phase of research that present the results of NASA programs and include extensive data or theoretical analysis. Includes compilations of significant scientific and technical data and information deemed to be of continuing reference value. NASA counterpart of peer-reviewed formal professional papers, but having less stringent limitations on manuscript length and extent of graphic presentations.
- **TECHNICAL MEMORANDUM.** Scientific and technical findings that are preliminary or of specialized interest, e.g., quick release reports, working papers, and bibliographies that contain minimal annotation. Does not contain extensive analysis.
- **CONTRACTOR REPORT.** Scientific and technical findings by NASA-sponsored contractors and grantees.

- **CONFERENCE PUBLICATION.** Collected papers from scientific and technical conferences, symposia, seminars, or other meetings sponsored or co-sponsored by NASA.
- **SPECIAL PUBLICATION.** Scientific, technical, or historical information from NASA programs, projects, and missions, often concerned with subjects having substantial public interest.
- **TECHNICAL TRANSLATION.** English-language translations of foreign scientific and technical material pertinent to NASA's mission.

Specialized services that complement the STI Program Office's diverse offerings include creating custom thesauri, building customized databases, organizing and publishing research results ... even providing videos.

For more information about the NASA STI Program Office, see the following:

- Access the NASA STI Program Home Page at <http://www.sti.nasa.gov>
- E-mail your question via the Internet to [help@sti.nasa.gov](mailto:help@sti.nasa.gov)
- Fax your question to the NASA STI Help Desk at (301) 621-0134
- Phone the NASA STI Help Desk at (301) 621-0390
- Write to:  
NASA STI Help Desk  
NASA Center for AeroSpace Information  
7115 Standard Drive  
Hanover, MD 21076-1320

NASA/TM-2007-214881  
ARL-TR-3883



# Analysis of the Effects of Sea Disposal on a One-Ton Container

*Wade C. Jackson*  
*U.S. Army Research Laboratory*  
*Vehicle Technology Directorate*  
*NASA Langley Research Center, Hampton, Virginia*

*Karen E. Jackson and Edwin L. Fasanella*  
*NASA Langley Research Center, Hampton, Virginia*

*John Kelley*  
*U.S. Army Research Laboratory*  
*Weapons and Materials Research Directorate*  
*Aberdeen Proving Ground, Maryland*

National Aeronautics and  
Space Administration

Langley Research Center  
Hampton, Virginia 23681-2199

July 2007

The use of trademarks or names of manufacturers in the report is for accurate reporting and does not constitute an official endorsement, either expressed or implied, of such products or manufacturers by the National Aeronautics and Space Administration or the U.S. Army.

Available from:

NASA Center for AeroSpace Information (CASI)  
7115 Standard Drive  
Hanover, MD 21076-1320  
(301) 621-0390

National Technical Information Service (NTIS)  
5285 Port Royal Road  
Springfield, VA 22161-2171  
(703) 605-6000

# Contents

Abstract.....	1
Introduction.....	1
Summary.....	2
Appendix A: Corrosion Assessment of a One-Ton Container	
Introduction.....	A1
Application of Previously Reported Data.....	A1
Velocity Effects.....	A4
Case Study.....	A4
Summary.....	A5
Proposed Work.....	A5
References.....	A5
Appendix B: Structural Buckling Analysis of a One-Ton Container using a Geometrically Nonlinear Shell Analysis Code (STAGS®)	
Summary.....	B1
Introduction.....	B1
Tank Properties and Dimensions.....	B2
Material and Structural Response.....	B3
Ocean Hydrostatic Pressure.....	B3
Finite Element Model.....	B3
Applied Pressure.....	B5
Linear Analysis.....	B6
Deformations.....	B6
Bifurcation-Buckling Analysis (Eigenanalysis).....	B7
Stress Analysis.....	B8
Critical Pressures and Depths.....	B11
Nonlinear Analysis with Initial Imperfections.....	B11
Buckling Analysis.....	B11
Stress Analysis.....	B12
Critical Pressures and Depths.....	B14
Effects of Internal Pressure.....	B16
Post-Yielding Response.....	B18
Additional Potential Leakage Sources.....	B19
Concluding Remarks.....	B19
References.....	B20
Appendix BA: Buckling Mode Shapes.....	BA1
Appendix C: Simulations of a One-Ton Container Exposed to External Pressure Using an Explicit, Transient Dynamic, Finite Element Code (LS-DYNA®)	
Introduction.....	C1
Container Model.....	C2
Simulations of Internal Contents and Impact.....	C4
Analytical Predictions - No Internal Contents.....	C4
Concluding Remarks.....	C8
References.....	C8

## Abstract

*Excess and obsolete stocks of chemical warfare material (CWM) were sea disposed by the United States between 1919 and 1970. One-ton containers were used for bulk storage of CWM and were the largest containers sea disposed. Disposal depths ranged from 300 to 17,000 feet. Based on a Type D container assembly drawing, three independent analyses (one corrosion and two structural) were performed on the containers to address the corrosion resistance from prolonged exposure to sea water and the structural response during the descent. Corrosion predictions were made using information about corrosion rates and the disposal environment. The structural analyses employed two different finite element codes and were used to predict the buckling and material response of the container during sea disposal. The results of these investigations are summarized below. Detailed reports on each study are contained in the appendices.*

## Introduction

Between 1919 and 1970, the United States sea disposed of excess, obsolete and unserviceable chemical warfare material. Disposal sites are in both the Atlantic and Pacific Oceans with depths ranging from 300 to 17,000 ft. below sea level (bsl). The disposal methods varied from loose disposal of individual items to consolidation in hulks and sinking. Corrosion from prolonged exposure will ultimately result in the failure of the containers. An assessment of corrosion was completed to determine if earlier estimates on the rate of corrosion could be supported. In addition, an evaluation was performed to determine if the one-ton containers might have failed during disposal due to hydrostatic pressures.

A Type D one-ton container was analyzed to determine its structural response during sea disposal and long-term corrosion resistance. The sea disposal analysis included structural buckling and material yielding due to the high external hydrostatic pressure. The Type D one-ton container has an internal volume of approximately 192 gallons and is 81.5 in. in length with a 30-in. diameter. Figure 1 shows a 1937 assembly drawing of the container. The container weighs approximately 1,600 lbs empty and has a maximum gross weight of 3,500 lbs. The tanks are filled with a liquid to approximately 90% of the volume. The tank is cylindrical with concave hemispherical end caps attached using a forge lap weld. The failure of the welded region was not considered due to a lack of information. The container is constructed from hot-rolled steel with a 0.41-in.-thick cylindrical wall and 0.75-in.-thick end caps. As a safety measure, three plugs are installed in each end cap and are designed to rupture at 500 psi of internal pressure. In the following analyses, the material properties were estimated since the exact properties of the steel were not known. After the completion of the analyses, a federal material specification, QQ-S-636, was deciphered from the assembly drawing and obtained. Although the material properties were not listed in the specification, the chemical composition was listed. The chemical composition specifies a maximum of 0.20% Carbon, 0.60% Manganese, 0.06% Phosphorus, and 0.06% Sulfur. This chemical composition is consistent with an AISI 1020 steel. Additional literature searches will be required to determine the material properties from this time period for the specified thicknesses.

Three studies were performed to assess the integrity of the one-ton container following sea-disposal: a corrosion assessment and two independent structural analyses. The corrosion assessment (Appendix A) was performed at the Weapons and Materials Research Directorate of the U.S. Army Research

Laboratory. A previous corrosion assessment, published in 1973, estimated the time to penetration to be 539 years. Since that study, a better understanding of deep-sea corrosion has developed. Using the new information and a better knowledge of the deep-sea environment, the time to penetration was reassessed assuming a similar site. The other two analyses, performed at NASA Langley Research Center, used finite element codes to predict the structural response during loose or “over the side” sea disposal. As discussed in Appendix B, the container was analyzed using STAGS®, a geometrically nonlinear shell analysis code developed to analyze buckling and post-buckling behavior. Using this code, the stresses and buckling response from applied hydrostatic pressure on the container were evaluated with and without geometric imperfections. As discussed in Appendix C, an explicit, transient dynamic, finite element code (LS-DYNA®) was used to simulate the effects of increasing hydrostatic pressure on the container. In addition, methods to simulate the internal contents of the tank and the impact with the ocean floor were investigated.

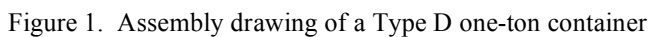
## Summary

Appendix A addresses the corrosion resistance of the containers. A previous assessment, published in 1973, estimated the time to penetration of the one-ton container with continuous exposure to seawater to be 539 years for a depth of 5600 ft. in the Pacific Ocean. Since this report did not include any supporting data, this estimation was reevaluated and found to be optimistic. Under uniform corrosion conditions, times to perforation were estimated to be between 80 and 300 years depending on dissolved oxygen concentrations. Water currents, biological effects, contact with dissimilar metals and the exact water chemistry at the site of disposal may further accelerate the corrosion rate. In some cases, a slight increase in seawater velocity can nearly double the corrosion rate. Current estimates for the Titanic, located 12,470 ft. below the surface of the Atlantic Ocean, indicate that the 0.75-in.-thick hull will last only 184 years. For the one-ton container, interactions of corrosion and hydrostatic stress may cause failures much sooner than corrosion alone. Because of the complexities of the factors involved, a significant amount of added effort may only slightly increase the confidence of the predictions. Additional literature searches on corrosion rates and conditions at known disposal sites, obtaining specific information on container materials and construction processes, obtaining specific information on the container coatings and processes, and locating additional comparison studies involving similar materials in the ocean may only somewhat reduce the uncertainty of the estimates.

The structural buckling (rapid collapse of the container) and container stresses were analyzed in Appendix B. STAGS® was used for the analysis and is a geometrically-nonlinear, finite element, shell analysis code which was specifically developed to analyze buckling and post-buckling behavior. Linear elastic properties were used to model the behavior of the steel. Initial yielding (permanent plastic deformation of the steel) was predicted using the maximum tensile stress. Since the actual yield stress was unknown, the yielding was bounded by a range of yield stresses for hot-rolled steel. Three competing mechanisms were examined that could result in a loss of structural integrity: structural buckling, yielding of the cylinder walls, and yielding of the end caps. Using a linear analysis, structural buckling was predicted to occur when the external pressure exceeded the internal pressure by 679 psi. For all analyses, the internal pressure was assumed to be 14.7 psi. Consequently, this buckling pressure corresponded to an ocean depth of 1520 ft bsl. The end caps were predicted to begin yielding for pressure differences of 577 to 1065 psi (1290 to 2390 ft. bsl), depending on the yield properties. Since dents and other geometric anomalies may significantly reduce the critical buckling pressure, geometrically nonlinear analyses were performed that included initial imperfections in the container geometry. To obtain the most severe cases, imperfection shapes were selected that corresponded to the buckling shapes from the linear analysis. The imperfection amplitudes studied were 1%, 10%, or 100% of the thickness of the cylinder wall. In general, the buckling pressure was not very sensitive to initial imperfections in the

container. Buckling pressures for imperfections with amplitudes less than 10% of the cylinder wall thickness were only slightly lower than the pressures from the linear analysis (no imperfections). The most severe case investigated was for an imperfection shape with three nodes around the circumference, and an amplitude equal to the cylinder wall thickness. For this case, the critical buckling pressure was reduced by 27% which corresponds to a depth of 1110 ft. bsl. For a container with an imperfection, either the end caps or the cylindrical section were predicted to begin yielding prior to buckling. The effect of the internal pressure was investigated by calculating the internal volume loss as a function of external pressure. This study showed that the container would begin yielding or buckle prior to any significant volume loss. For buckling calculations, internal pressure increases only need to be considered if a fluid occupies more than 99% of the container volume. Yielding may be beneficial if the container can collapse down to the fluid volume without a material failure. However, additional material and internal contents information are required to predict this post-buckling and post-yielding behavior. The vent plugs (if left installed), valve threads, and the forge weld attaching the end caps may be susceptible to leakage during descent and should be analyzed further.

The structural response of the container to an external pressure was simulated using an explicit, transient dynamic, finite element code (LS-DYNA®) in Appendix C. An LS-DYNA® finite-element model of the cylindrical container containing 9,752 shell elements was created. The model was analyzed without the internal contents to determine the buckling load for the externally applied pressure. The LS-DYNA® simulation predicted that initial buckling would occur for an external pressure of 699.2 psi. This value is only 3% higher than the buckling pressure predicted by the STAGS® simulation (679 psi) described in Appendix B. Two methods to simulate the internal contents were investigated. In the first method, the interior was filled with solid elements that were assigned a material property that mimicked the ideal gas law for pressure as a function of volumetric strain. The internal pressure was not significant until the interior volume of the container was reduced to near the fluid volume. This reduction in container volume requires yielding in the container. Consequently, the predictions are highly dependent on the tensile and compressive material properties to failure of the container, as well as the properties of the internal contents. Since these properties were not available, the results from this analysis are not presented. In the second method to simulate the internal contents, a coupled fluid-structure interaction simulation was investigated using the Arbitrary Lagrange Euler (ALE) formulation within LS-DYNA®. A model to simulate the impact with the ocean floor was also created. This model included the external pressure, the internal contents, and the impulsive loading simulating the impact. Since this model is also very dependent on specific failure data and properties, no results are presented.



# Appendix A: Corrosion Assessment of a One-Ton Container

John Kelley  
U.S. Army Research Laboratory  
Weapons and Materials Research Directorate  
Aberdeen Proving Ground, Maryland

## Introduction

This appendix addresses the corrosion resistance of the containers at a depth of 5000 ft. beneath the Pacific Ocean. A report published in 1973 by US Army Munitions Command [1] describes the behavior of chemical agents exposed to various environmental conditions. The report also includes a table in the appendix which lists estimated times to penetration by corrosion of 11 different munitions and containers at a depth of 5600 ft. (1700 meters) in the Pacific Ocean. In the table, the one-ton container is estimated to last 539 years before corrosion will penetrate the thinnest section of the wall. The report, however, did not include any data to support that estimate. Further, interactions of corrosion and hydrostatic stress may cause failures much sooner than corrosion alone and will not be considered in this analysis. The purpose of this section is to attempt to determine if the 539 years is a reasonable estimate for the corrosion life of these containers.

## Application of Previously Reported Data

There are several factors that influence the corrosion rate in deep water. They are: water temperature, dissolved oxygen, water current velocity, biological effects, and galvanic effects among others. Although all factors should be considered, some assumptions were made in order to expedite this investigation:

1. Galvanic effects will be neglected because the amount of cathode (brass plugs and valve) is considered insignificant compared to that large anode (steel containers)
2. Biological effects will be neglected at this time
3. The tanks are made from uncoated carbon steel
4. The thinnest section of the one-ton container = 0.41 inches (0.010414 meters) [2]
5. All were disposed of in the Pacific Ocean
6. The average depth at the site of disposal is approximately 5000 ft. bsl (1500 meters)

Using Figure A1 and Table A1, we can further assume the following [3]:

7. The temperature at the ocean floor is between 36 and 41 degrees F (2 and 5 degrees C)
8. The dissolved oxygen is between 0.0005 and 0.003 ft<sup>3</sup>/ft<sup>3</sup> (0.5 and 3.0 mL/L)

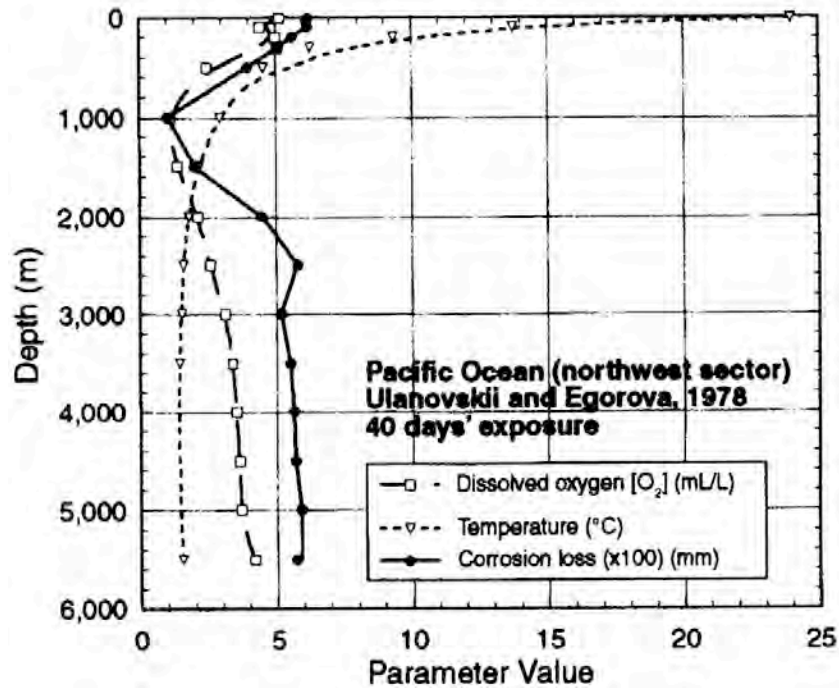


Figure A1. Dissolved oxygen (DO), temperature (T), and corrosion loss at a site in the Pacific Northwest. [3]

The dissolved oxygen concentration and the seawater temperature are the more predominant factors for determining corrosion rates in deep-sea environments. However, literature shows that the presence of dissolved oxygen (DO) appears to be the most significant. The amount of dissolved oxygen has been reported to have a nearly linear relationship with corrosion loss [2, 5]. It has been reported that in some eastern and western Pacific Ocean sites the DO concentrations at depths greater than 3300 feet (1000 meters) are much lower than at the surface and may be as low as 0.001 ft<sup>3</sup>/ft<sup>3</sup> (1 mL/L) [2].

Presented in Table A1 is a list of empirical data taken from a surface study [4] conducted at Wrightsville Beach and a deep-sea study in the Pacific Ocean. The study considered the effects of such parameters as dissolved oxygen concentration, salinity, temperature, and pH. Equation 1 was derived from this study and, as mentioned in the test, is limited to the areas where the study was conducted. However, by assuming that there will be little difference in these parameters (pH and Salinity) in the Pacific water, and by using the assumptions established earlier, an estimate of the deep-water corrosion rate can be made. These corrosion rates can be seen in Figure A2.

Table A1: Corrosion Rates of Carbon Steel for Near-Surface and Deep-Sea Immersion [4]

Immersion depth		Temperature, °C	Oxygen concentration, ppm	Immersion time, days	Corrosion rate	
m	ft				µm/yr	mil/yr
Near-surface site (a)						
...	...	5 to 30	5 to 10	365	130	5.0
Deep-sea site (b)						
715	2340	7.2	0.6	197	43	1.7
1615	5300	2.5	1.8	1604	23	0.9
1720	5640	2.8	1.2	123	50	2.0
		2.3	2.1	751	20	0.8
2065	6780	2.7	1.7	403	58	2.3
(a) Wrightsville Beach NC. (b) Pacific Ocean.						

$$CR = 21.3 + 25.4DO + 0.356T \quad (1)$$

Where: CR = Estimated Corrosion Rate (µm)

DO = Dissolved Oxygen Concentration (mL/L)

T = Water Temperature (°C)

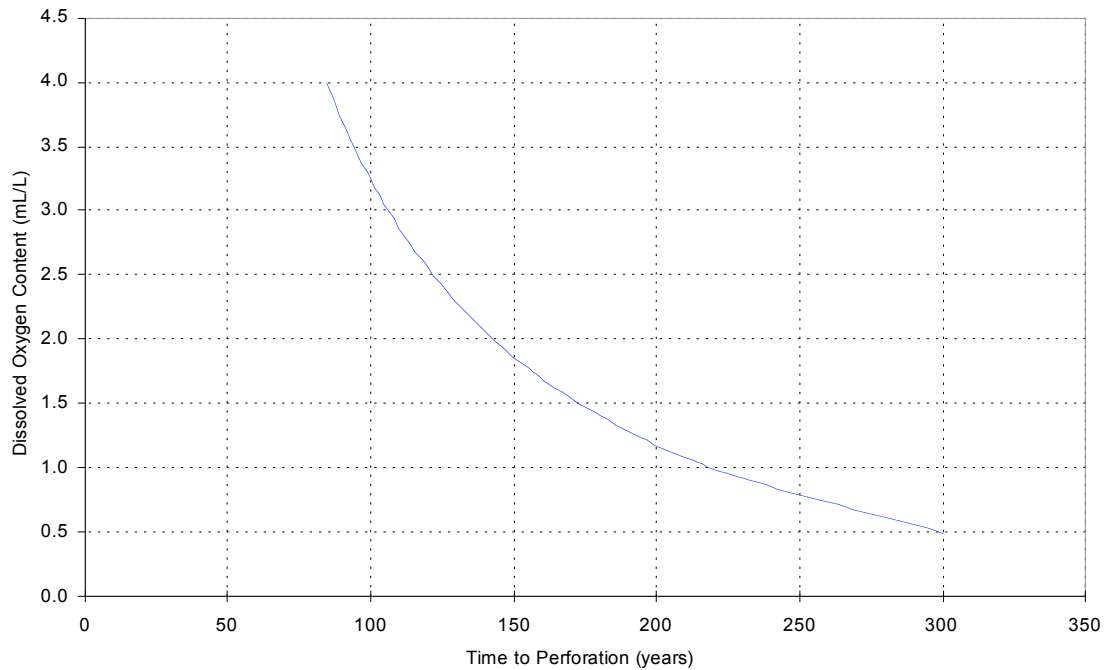


Figure A2. Corrosion penetration of a 0.41 inch (0.010414 meters) thick carbon steel container in 36 degrees F (2 degrees C) seawater. Plotted using Eq. 1, Metals Handbook Vol. 1 9<sup>th</sup> ed., pg 739. Calculations do not consider water current velocity.

## Velocity Effects

An increase in the seawater velocity will typically increase the rate of corrosion of steel. The effect is twofold: 1) the steady flow of water acts to provide a constant supply of dissolved oxygen to the steel 2) the moving water helps to release some of the protective oxide allowing the oxygen to come in contact with the steel. However, given the unique conditions in deep-water atmospheres (low DO and temperatures, and anaerobic bacteria growth), it is unclear at this time what the magnitude of the increase would be. There has been work done to study the effects of velocity on the corrosion of steel. Figure A3 is the result of one such study showing the effects of the velocity of seawater at ambient temperature. It is evident that the relationship between the velocity effect and corrosion rate is nearly linear at lower velocities. In fact, Figure A3 shows that in some cases, with a slight increase in velocity the rate of corrosion can nearly double.

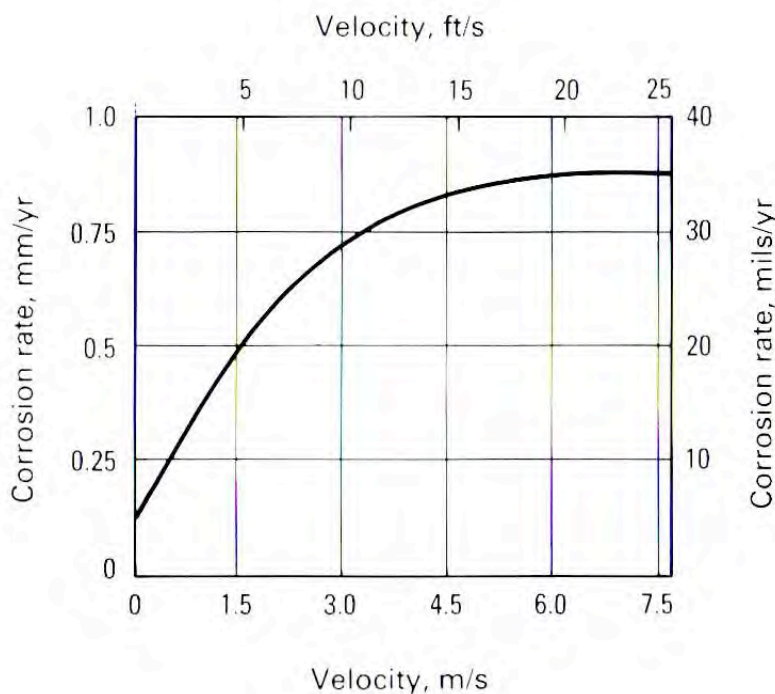


Figure A3: Effect of velocity on the corrosion of steel by seawater at ambient temperature. [5]

## Case Study

Since it sank in 1912, the Titanic has been one of the most studied shipwrecks in history. The ship was also constructed from carbon steel similar to AISI 1020 with a chemical composition that specifies a maximum of 0.20% Carbon, 0.47% Manganese, 0.045% Phosphorus, and 0.069% Sulfur [6]. Several observations of the Titanic have revealed corrosion products known as rusticles. It is thought that these rusticles are caused by iron consuming bacteria that grow rapidly under anaerobic (no oxygen) conditions [7]. Although it is corroding slower than first anticipated, some corrosion experts predict that the vessel will collapse on itself in about another 75-90 years [8]. If that prediction is true, the Titanic will have lasted between 169 to 184 years. However, the Titanic is located 3800 m (12,470 ft) below the surface of the Atlantic Ocean, which has somewhat different chemistry than the Pacific Ocean. Thus, the exact effect the anaerobic bacteria will have on the one-ton containers in the Pacific Ocean is unknown at this

time and will be neglected for this comparison. But it should be understood that biological effects would likely accelerate the degradation of the steel.

## Summary

Based on empirical data found in the literature, the case study presented, and using the derived equation, it appears that the 539 years to perforation by corrosion reported in Epstein et al [1] is considered somewhat optimistic. It is more likely that the one-ton containers would have corroded through in far less time. Figure A2 is an estimate of some times to perforation under uniform corrosion conditions with a known water temperature and known dissolved oxygen concentrations. These estimates, however, neglect several important factors including sediment cover, water current velocity, biological effects and the exact water chemistry at the site of disposal, which can influence the corrosion process and cause significant acceleration of corrosion rates. The case history of the Titanic serves to illustrate what happens to a carbon-steel vessel in deep seawater after nearly 100 years. The average thickness of the hull of the Titanic was originally 0.75 inches (0.01905 meters), and it is predicted to last about 184 years. Even so, this estimate is still quite rough, as scientists are still learning about this new phenomenon, which produced rusticles on the Titanic and influences the corrosion rate. Therefore, making a corrosion rate estimate for the ton-containers is especially difficult given that many of the conditions at each individual disposal site are unknown. Because of the nature of deep-water corrosion, it is very difficult to tightly bracket the life expectancy with a high degree of confidence. In fact, a significant amount of added effort may only slightly increase the confidence of the prediction.

## Proposed Work

Because of the nature of deep-water corrosion, it is very difficult to tightly bracket the life expectancy with a high degree of confidence. In fact, a significant amount of added effort may only slightly increase the confidence of the prediction. If improved corrosion estimates are needed, ARL proposes the following at a minimum: 1) A thorough survey of literature on the topic of deep-water corrosion in the ocean in order to learn more about the specific characteristics. Mappings of salinity, water temperature, biological makeup, dissolved oxygen content and ocean currents could be applied to this examination to calculate the corrosion rates in various oceans. 2) Although the general construction of the one-ton containers is known, a more specific account of the materials, construction techniques and processes (welding process, mill scale present, etc.) is needed. All of these can affect the rate of corrosion. 3) It is likely that the one-ton containers were coated with either an organic, or inorganic coating, or a combination of the two coating types. Coatings have been known to cause preferential corrosion (if damaged) as well as protect structures from corrosion. Much of it depends on the types of coatings and processes used, and if the coating was damaged when the one-ton containers were disposed. Therefore, it is important to know the types of coatings and processes, and the relative age and condition prior to disposal. 4) Finally, as can be seen by the example of the Titanic, “real world” case studies are invaluable in understanding some of the extraordinary circumstances present beneath the ocean. For this reason, a more comprehensive literature review of these types of case studies involving similar materials (such as with shipwrecks) should be performed.

## References

1. Epstein, Joseph, Rosenblatt, David H., “Summary Report on a Data Base for Predicting Consequences of Chemical Disposal Operations,” US Army Munitions Command, Edgewood Arsenal, Edgewood MD, Jan. 1973.
2. SciTech Services Inc “HD ton Container Survey (Pressurization and Plug/Valve Integrity) Historical Review Final Report,” March 29, 1996.

3. Melchers RE, "Effect of Immersion Depth on Marine Corrosion of Mild Steel," Corrosion 61, 2005.
4. American Society for Metals, Metals Handbook 9<sup>th</sup> ed., Vol 1, "Properties and Selection of Irons and Steels," pp. 739-746.
5. American Society for Metals, Metals Handbook 9<sup>th</sup> ed., Vol 13, "Corrosion," pp. 333, 516.
6. Katherine Felkins, H.P. Leighly, Jr., and A. Jankovic, "The Royal Mail Ship Titanic: Did a Metallurgical Failure Cause a Night to Remember?" <http://www.tms.org/pubs/journals/JOM/9801/Felkins-9801.html>
7. The Titanic Nautical Society and Resource Center, <http://www.titanic-nautical.com>.
8. Information obtained from the Corrosion Doctors Web Site, <http://www.corrosion-doctors.org/Landmarks/titan-corrosion.htm>.

# Appendix B: Structural Buckling Analysis of a One-Ton Container using a Geometrically Nonlinear Shell Analysis Code (STAGS<sup>®</sup>)

Wade C. Jackson  
U.S. Army Research Laboratory  
Vehicle Technology Directorate  
NASA Langley Research Center, Hampton, Virginia

## Summary

The effects of increasing hydrostatic pressure on a Type D one-ton container were investigated using the STAGS<sup>®</sup> structural analysis program. Finite element models of the complete container were created using MSC.Patran<sup>®</sup> for input into the STAGS<sup>®</sup> analysis code. The material properties or a range of material properties were obtained from the ASM Metals Handbook since the actual properties were unknown. Three competing structural and material responses were examined: structural buckling (rapid collapsing of the container), cylinder yielding, and end cap yielding. The maximum principal tensile stress was used to predict the yielding of the cylinder and the end caps. Using a linear analysis, structural buckling was predicted to occur when the external pressure exceeded the internal pressure by 679 psi. For all analyses, the internal pressure was assumed to be 14.7 psi. Consequently, this buckling pressure corresponds to an ocean depth of 1520 feet. However, the end caps were predicted to begin yielding between 577 and 1065 psi (1290 to 2390 ft. bsl) depending on yield properties. Geometrically nonlinear analyses were performed that included the effects of initial imperfections in the container geometry. To obtain the most severe case, imperfection shapes were selected that corresponded to the mode shapes from the first and second eigenvalues. The amplitudes of the imperfections that were investigated were 1%, 10%, or 100% of the thickness of the cylinder wall. Buckling pressures from nonlinear analyses of imperfections with amplitudes of only 1% of the cylinder wall thickness were nearly identical to those from the linear results (no imperfections). The most severe case was an imperfection with the mode shape of the first eigenvalue with an amplitude equal to the cylinder wall thickness. For this case, the critical buckling pressure was reduced by 27%, which corresponds to a depth of 1110 ft. bsl. In general, the container was not sensitive to small initial imperfections in the geometry. Increases in the internal pressure caused by a reduction in the container volume due to the increasing hydrostatic pressure were not found to affect the predictions. For a container with an imperfection, either the end caps or the cylindrical section should experience localized yielding prior to structural buckling. Yielding may be beneficial if the internal volume can be reduced to near the fluid volume prior to a material failure. However, additional material and container information is required to predict this post-buckling and post-yielding behavior. The forge welds used to attach the end caps are critical but were not analyzed due to a lack of information. In addition, other potential sources of leaking such as the valve threads and the safety vents (if left in place during sea disposal) should be investigated.

## Introduction

A Type D one-ton container was analyzed using the STAGS<sup>®</sup> (SStructural Analysis of General Shells) finite element [1] program to determine the material and structural response during sea disposal.

Structural buckling (rapid collapsing of the container) due to the high external hydrostatic pressure was considered the primary threat. Figure 1 (main section of report) shows the assembly drawing of the container from 1937. Finite element models of the entire container were created based on this assembly drawing using the MSC.Patran® finite element modeling software [2]. Finite element models with two different mesh sizes were created to confirm the convergence of the model. The STAGS® finite element program was used to analyze the buckling and evaluate the container stresses caused by the hydrostatic pressure. STAGS® is used extensively throughout the aerospace, shipbuilding and other industries for analysis of panels, pressure vessels, and general shell structures. STAGS® was specifically developed to perform geometrically nonlinear analyses of complex systems that includes the buckling and post-buckling regimes. Specific routines are included in STAGS® that allow initial geometric imperfections to be added to the model.

Initially, the Type D one-ton container was analyzed without an imperfection using a linear analysis to obtain the critical buckling pressures (eigenvalues) and associated mode shapes. A stress analysis was performed to determine the maximum stresses and their locations. Since cylinder buckling can be strongly affected by the presence of geometric imperfections, geometrically nonlinear analyses were performed on containers with assumed initial imperfections. Manufacturing defects, variations in thickness, and variations in material properties may also have a large influence on the buckling predictions but were not investigated. In the nonlinear analyses, the effects of two geometric imperfection shapes, corresponding to the first two eigenvalue mode shapes, were evaluated with three different amplitudes. An imperfection coinciding with the shape of a buckling mode should provide a “worst case” buckling value. No data were available on actual geometric imperfections, thickness variations, or manufacturing defects. Using the nonlinear analyses, the critical buckling pressure and container stresses were evaluated. Finally, an analysis was performed to determine the effects on the predictions of an internal pressure increase caused by a reduction in the cylinder’s internal volume due to the hydrostatic pressure.

## Tank Properties and Dimensions

The Type D one-ton container is a cylindrical tank  $81.5 \pm 0.5$  inches long with an outside diameter of  $30.0 \pm 0.5$  inches. An assembly drawing of the tank is shown in Figure 1 of the main section of this report. On this drawing, the container material is specified as hot-rolled steel in the “as-rolled” condition with minimum wall thicknesses of 13/32 (0.406) inches for the cylindrical section and 3/4 (0.75) inches for the hemispherical end caps. Since the actual steel properties for the containers were not known, the properties for this analysis were obtained for hot-rolled steel from the ASM Metals Handbook [3] and are listed in Table B1. Depending on the thickness, quality and composition of the steel, the yield and tensile strengths can vary greatly as given by the ranges in Table B1.

Table B1. Properties of Hot-Rolled Steel

	E, msi	$\nu$	Yield strength range, ksi	Tensile strength range, ksi
Hot-Rolled Steel	29.0	0.29	26-48	40-67

The internal volume of the cylinder was calculated based on the dimensions given in the assembly drawing. The container volume was calculated as the volume of the hemispherical end caps ( $V_{endcap}$ ) subtracted from the volume of the cylindrical portion ( $V_{cylinder}$ ) and is given in equation 1

$$V_{\text{tank}} = V_{\text{cylinder}} - 2V_{\text{endcap}} = \pi r_i^2 l - 2 \left[ \frac{1}{6} \pi h (3r_i^2 + h^2) \right] \quad (1)$$

where the inner cylindrical radius ( $r_i$ ) equals 14.59 inches, the internal cylinder length ( $l$ ) equals 72.1 inches, and the height of the hemispherical section ( $h$ ) equals 3.78 inches. The calculated volume was 45680 in<sup>3</sup> which equals 26.43 ft<sup>3</sup> or 197.7 gallons.

## Material and Structural Response

This analysis considers three competing material and structural responses as the hydrostatic pressure increases: buckling (rapid collapse of the container walls), yielding in the cylindrical section, and yielding in the hemispherical end caps. Any of these three responses may cause a significant loss of structural integrity. For ductile materials such as low-carbon steels, the onset of yielding in tension is often used to predict structural failure. Using this criterion typically provides a conservative material failure prediction. A more sophisticated material and failure model is required to predict the failure after yielding has occurred and would require specific material properties that were unavailable. Yielding may accelerate buckling and reduce the critical buckling pressure. Low-carbon steels have a maximum elongation at failure of 20 to 40%. Yielding could be beneficial if the internal volume could be reduced by the amount of the gas volume before a material failure occurs. Consequently, the internal and external pressures would equalize to limit further structural damage. In this analysis, yielding was predicted when the maximum principal tensile stress exceeded the yield stress. When loaded in compression, structures made from ductile materials will typically buckle before reaching the compressive failure strength of the material. Consequently, compressive stresses were used for buckling computations and not compressive fracture analyses.

## Ocean Hydrostatic Pressure

The density of ocean water varies only slightly with temperature (greatest sensitivity), salinity, and pressure. The density near the surface is approximately 0.03703 lbm/in<sup>3</sup> (1.025 g/cm<sup>3</sup>) but is relatively constant at (0.03714 lbm/in<sup>3</sup>) 1.028 g/cm<sup>3</sup> below 3000 feet. For this analysis, a constant value of 0.03714 lbm/in<sup>3</sup> (1.028 g/cm<sup>3</sup>) was used. The hydrostatic pressure was calculated as:

$$P_{\text{total}} = P_{\text{atm}} + \rho gh \quad (2)$$

where  $P_{\text{total}}$  is the hydrostatic pressure,  $P_{\text{atm}}$  is the atmospheric pressure,  $\rho$  is the density of seawater,  $g$  is the acceleration due to gravity, and  $h$  is the depth. For the initial analyses, the pressure difference was held constant and independent of container deformations. The initial internal pressure was assumed to be atmospheric. Consequently, the relative pressure ( $P_{\text{total}} - P_{\text{atm}}$ ) was simply  $\rho gh$ .

## Finite Element Model

A STAGS® [1] finite element model of the full tank was created using MSC.Patran® [2] based on the dimensions in the assembly drawing (Figure 1 of main report). The exterior hemispherical cover for the valves was not included in the model since it is not a structural part. The holes for the valves and vent plugs were not modeled since they are filled. “Classic” four-node quadrilateral shell elements (STAGS® E410) were used to model the container walls. The surface contours in the model were created to match the interior contours of the tank, which simplified the model in the region where the hemispherical end caps are welded to the cylinder wall. An eccentricity was supplied to the shell

properties to account for the offset of the mid-plane of the container walls from the reference surface. A similar approach was used in the welded region where the joint is represented by a wall thickness of 1.156 inches (combined cylinder and end cap thickness) with an eccentricity. The geometry of the region around the lap weld was not precisely defined in the assembly drawing. Consequently, a computer program was used to extract data points along the interior contours of this joint from an image of the assembly drawing. The coordinates of these points were then used to generate a spline in MSC.Patran®. The reference surface for this region is shown for this cross section in Figure B1. After a quadrant of the cross-sectional geometry was generated in MSC.Patran®, this quadrant was mirrored then rotated 360° to obtain the full 3D geometry.

Two finite element models were generated with 48 and 96 shell elements around the circumference, which corresponded to nominal element edge lengths of 2 inches and 1 inch, respectively. An example of the mesh with 48 elements around the circumference is shown in Figure B2. These two models were used to verify the solution convergence. The boundary conditions consisted of fixing the displacements of three nodes on the perimeter of the end caps. The top node on the “+x” end cap was fixed in the x, y, and z directions. On the “-x” end cap, the top node was fixed in the y and z directions, and the bottom node was fixed in only the z direction.

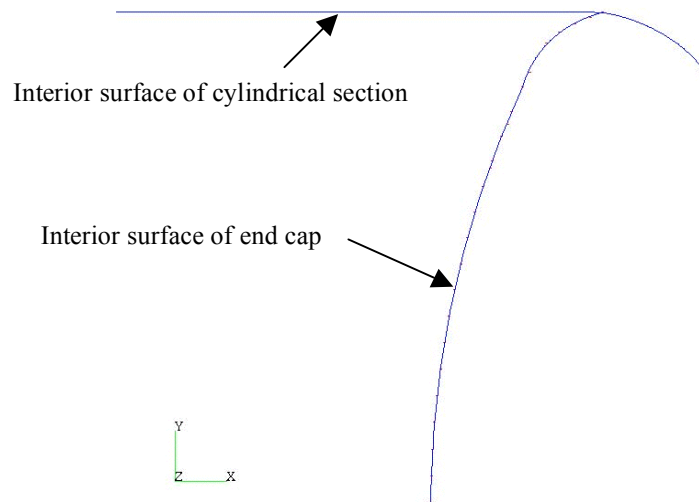


Figure B1. Cross section of inner surface geometry.

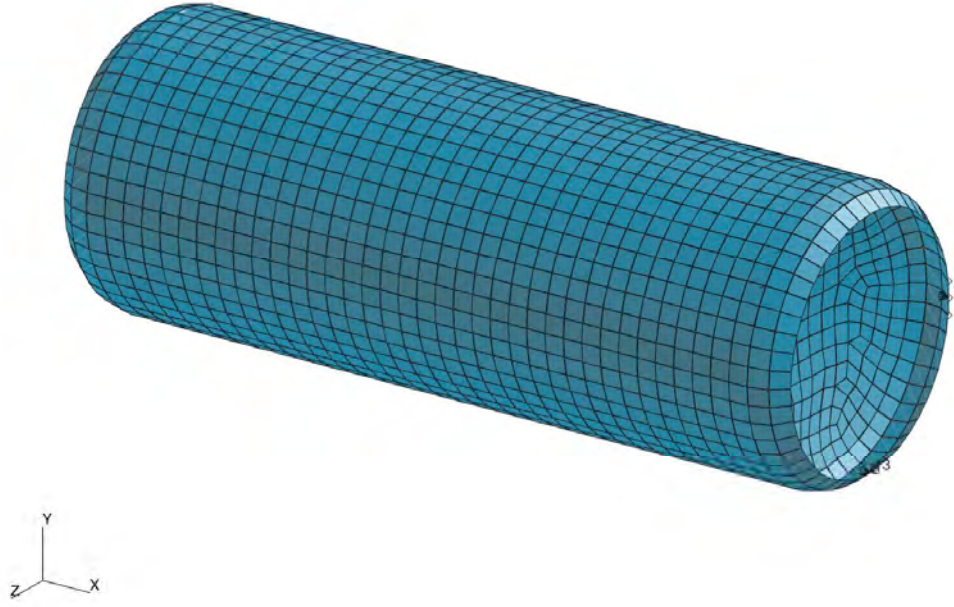


Figure B2. An MSC.Patran® model of the container with 2-inch-square elements.

## Applied Pressure

A “live” hydrostatic pressure was applied at the reference surface. A ‘live’ pressure loading option maintains the pressure normal to the deformed surface throughout geometrically nonlinear deformations. A slight discrepancy was created since the actual hydrostatic pressure is applied to the exterior surface instead of the interior reference surface. Since the hoop stresses are twice the magnitude of the axial stress, an equivalent exterior pressure was calculated based on equivalent hoop stresses. The hoop stress at any given location in a simple cylinder due to internal and external pressures is given by equation 3 [4].

$$\sigma_{hoop} = \frac{P_i r_i^2 (r_o^2 + r^2) - P_o r_o^2 (r_i^2 + r^2)}{r^2 (r_o^2 - r_i^2)} \quad (3)$$

where  $P_i$  is the interior pressure,  $P_o$  is the exterior pressure,  $r_i$  is the inner radius,  $r_o$  is the outer radius, and  $r$  is the radial position for the stress calculation. The hoop stress on the interior wall can then be calculated by setting  $r$  equal to  $r_i$  (equation 4).

$$\sigma_{hoop} = \frac{(r_i^2 + r_o^2) P_i - 2 r_o^2 P_o}{r_o^2 - r_i^2} \quad (4)$$

An equivalent exterior pressure,  $P_o$ , can then be obtained by matching the hoop stress produced by an interior pressure with the hoop stress produced by an exterior pressure. This relationship is shown in equation 5 and produces an equivalence factor of -0.973 or an interior pressure of -1.000 psi produces the same interior surface hoop stress as 0.973 psi of an exterior pressure.

$$P_o = -\frac{r_i^2 + r_o^2}{2r_o^2} P_i \quad (5)$$

Similarly for the axial stress, the stress differs for a pressure applied to an interior or exterior surface (equation 6).

$$\sigma_{axial} = \frac{P_i r_i^2 - P_o r_o^2}{r_o^2 - r_i^2} \quad (6)$$

An equivalent exterior pressure is obtained by matching the axial stresses for an internal and external pressure (equation 7).

$$P_o = -\frac{r_i^2}{r_o^2} P_i \quad (7)$$

For the geometry in this case, the equivalence factor is 0.947 or an interior pressure of -1.000 produced the same axial stress as an external pressure of 0.947 psi. As stated previously, the factor obtained from the hoop stress calculation (0.973) was used since the hoop stress is approximately twice as large as the axial stress, and the buckling deformations are primarily in the hoop direction.

## Linear Analysis

### Deformations

A linear analysis was initially performed to investigate the deformations and verify the model. An example of a deformed mesh is shown in Figure B3 for an equivalent external pressure of 0.973 psi (1.000 psi of internal pressure). Along the cylindrical section, the primary deformation is a uniform inward contraction of the cylinder. A small transition region exists near the end caps where the cylinder walls rejoin the end caps. The normal deformations are significantly larger for the end caps than for the cylindrical walls.

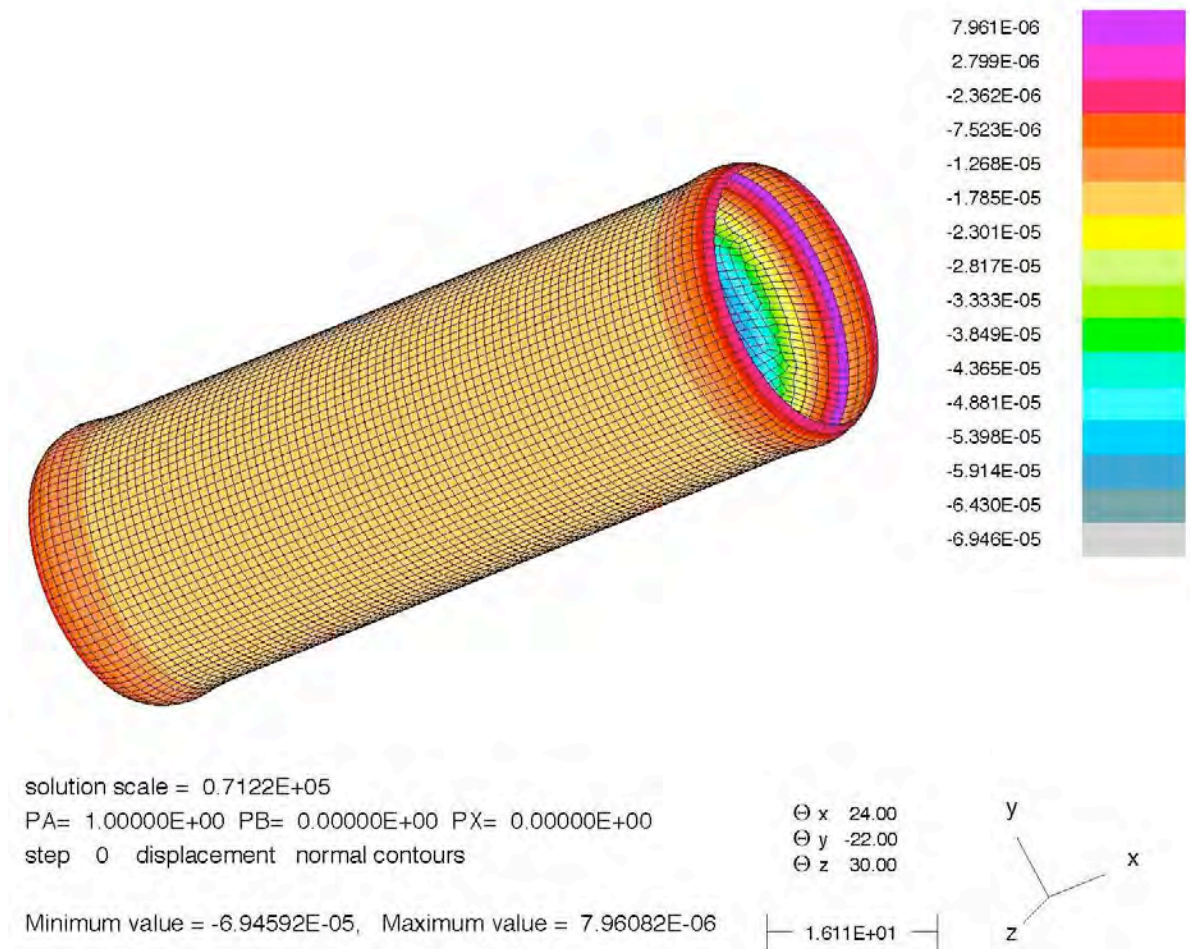


Figure B3. Normal displacement contours plotted on the deformed geometry from a linear analysis

## Bifurcation-Buckling Analysis

The first ten eigenvalues from a linear buckling analysis were obtained using STAGS®. Meshes with either 48 or 96 circumferential elements were used which corresponded to square elements with edge lengths of 2 or 1 inches, respectively. This analysis assumes no internal pressure changes due to container deformations. The critical external hydrostatic pressures associated with each eigenvalue are summarized in Table B2 along with the mode shapes. The number of half-waves in the longitudinal directions and full-waves in the circumferential directions are denoted by the parameters  $m$  and  $n$ , respectively. The mode shapes corresponding to these eigenvalues are shown in Appendix BA for the mesh with 1-inch square elements. The shape of the first (lowest) eigenvalue is different between the two meshes but represents only a 2.5% difference in the critical pressures. Several of the other eigenvalues also are associated with different mode shapes for the two meshes. However, the critical pressures associated with each eigenvalue are nearly identical for the two meshes. Also, for a given mesh, the critical pressures are almost identical for each pair of eigenvalues (i.e., 1-2, 3-4, etc.). The paired eigenvalues represent simple rotations of the same mode shape about the x-axis or nearly coincident buckling modes. The lowest critical buckling pressure (eigenvalue 1) of 679 psi corresponded to a pressure at 1520 ft. below sea level. For the 1-inch element mesh, two eigenvalues for the bifurcation loads are clustered near the lowest critical pressure. For all subsequent analyses, only the mesh with the 1-inch-square elements was used.

Table B2. Critical Buckling Exterior Pressures

Eigenvalue	2-inch elements		1-inch elements		
	Critical external pressure, psi	Buckling shape m, n	Critical external pressure, psi	Buckling shape m, n	Distance below sea level, ft
1	696	1, 3	679	1, 3	1520
2	696	1, 3	684	1, 2	1530
3	912	1, 4	911	1, 2	2040
4	912	1, 4	911	1, 4	2040
5	1374	1, 6	1370	1, 5	3070
6	1374	1, 5	1371	1, 5	3080
7	1443	2, 4	1443	2, 4	3240
8	1443	2, 4	1447	2, 4	3250
9	1614	2, 5	1612	2, 5	3620
10	1614	2, 5	1613	2, 5	3620

The geometry of the container can be idealized as a thin-walled cylinder with the ends closed and held circular. A formula [4] exists for this simplified geometry to calculate the critical buckling pressure for a uniform external pressure applied to both the ends and the cylinder wall. Using this formula, a critical pressure of 694 psi was calculated for a buckling geometry with three full waves around the circumference ( $n = 3$ ). This value is just 2.2% higher than the critical pressure calculated using STAGS® and supports the validity of the STAGS® predictions.

## Stress Analysis

The stresses in the container were evaluated to determine if the end caps or cylindrical walls might yield prior to the first buckling pressure eigenvalue. Initially for model verification purposes, the stresses obtained from the finite element analysis were compared to the closed-form values for a simple cylinder with closed ends subjected to external hydrostatic pressure. For this case, the hoop and axial stresses were calculated using the formulas given in equations 3 and 6, respectively. The ratio of hoop stress to axial stress is not exactly 2.0 due to the relatively low ratio of wall thickness to cylinder radius. These stresses were compared to the stresses obtained from the linear finite element analysis (Table B3) for an equivalent external pressure of 679 psi, which corresponds to the critical pressure associated with the first eigenvalue. The stresses calculated from the equations were within 2% of those obtained from the finite element analysis in the center section of the cylinder. Plots of the hoop and axial stress distributions for the inner surface are shown in Figures B5 and B6, respectively. The axial and hoop stresses are compressive and uniform in the cylindrical section but decrease slightly near the end caps. The shear stresses are negligible and are not presented.

Table B3. Comparison of Stresses from the Closed-Form and Finite Element Analyses.

Stress	Closed Form, Eqn. 3 or 6	Finite Element Analysis	Percent Difference
$\sigma_{\text{hoop}}$ , ksi	-25.4	-25.1	1.2
$\sigma_{\text{axial}}$ , ksi	-12.4	-12.5	0.8

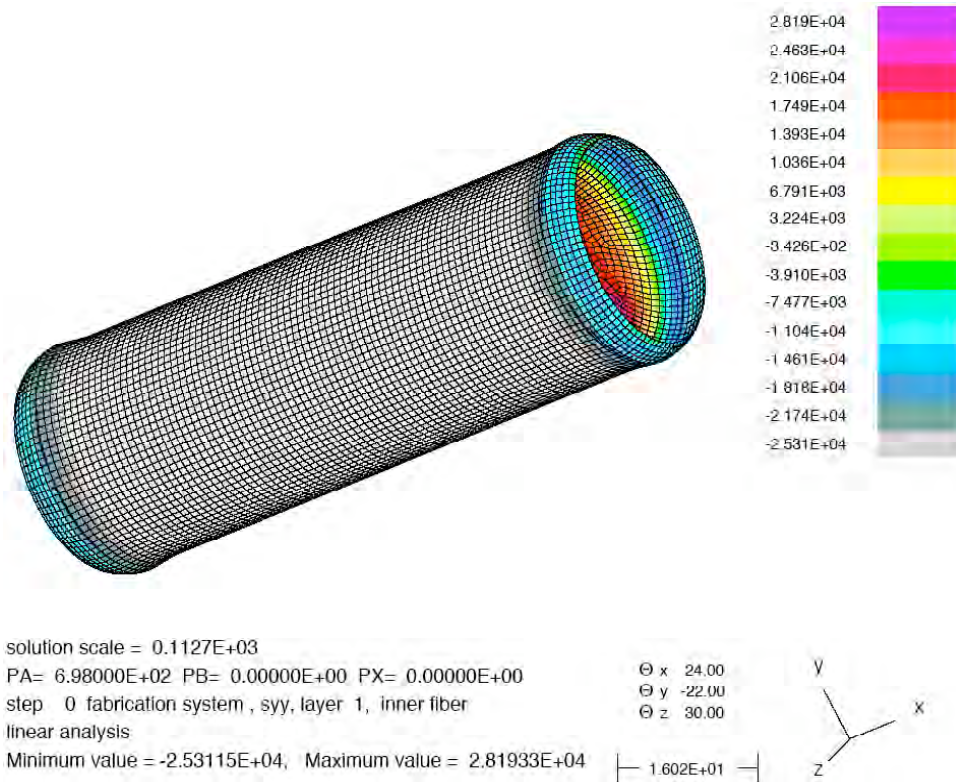


Figure B5. Hoop stress distribution at 679 psi.

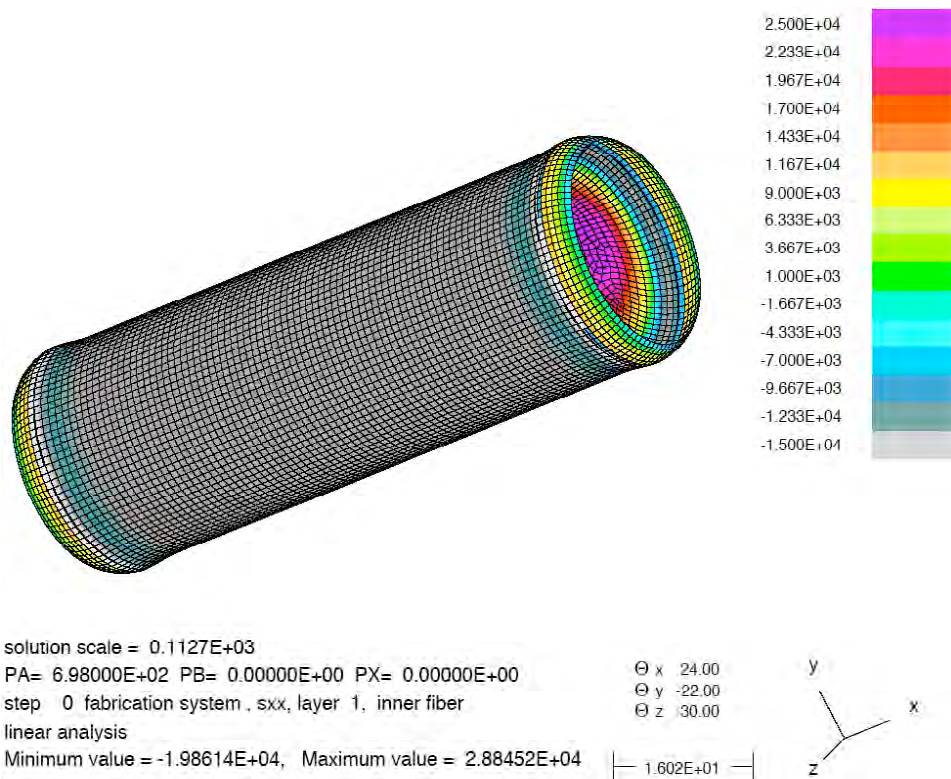


Figure B6. Axial stress distribution at 679 psi.

The hemispherical end caps have larger relative displacements and higher stresses than the cylindrical section of the container. Plots of the maximum principal stress are shown for the inner and outer surfaces of the container in Figures B7 and B8, respectively. On the inner surface, the maximum principal tensile stress is 29.6 ksi. A region of peak stress exists in a ring on the end cap that is located radially outward approximately 50% to 70% of the cylinder radius (Figure B7). On the exterior surface of the end cap, the maximum principal stress reaches 30.6 ksi. This area of peak stress exists adjacent to the welded region in the end cap.

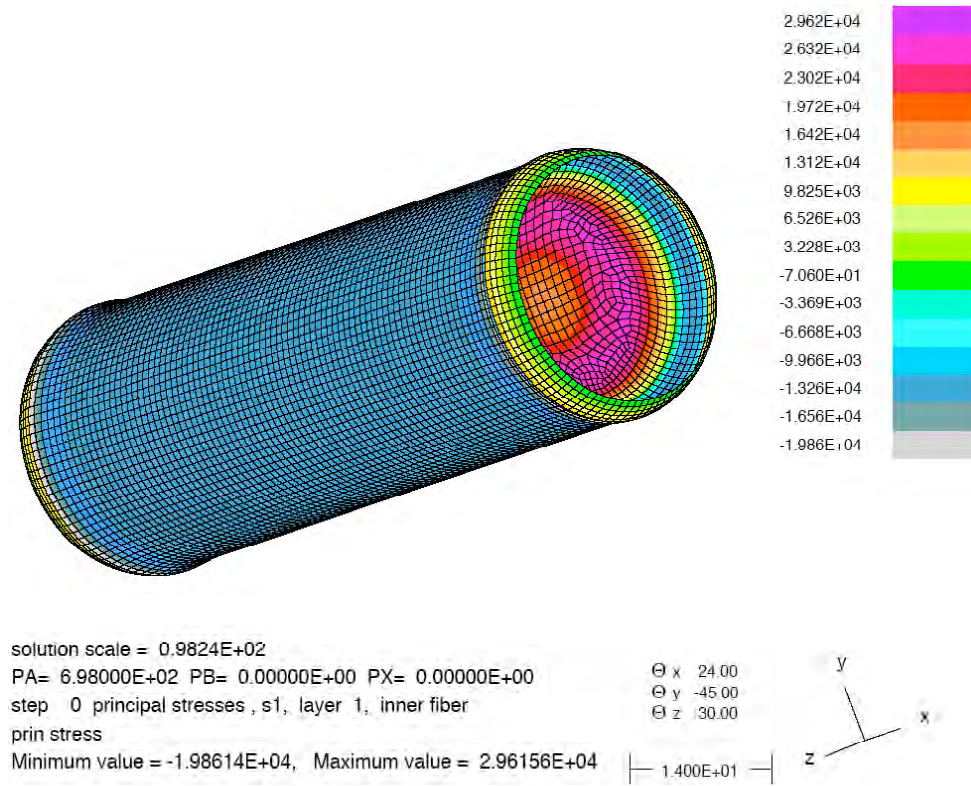


Figure B7. Principal Stress Distribution on the Interior Surface at 679 psi.

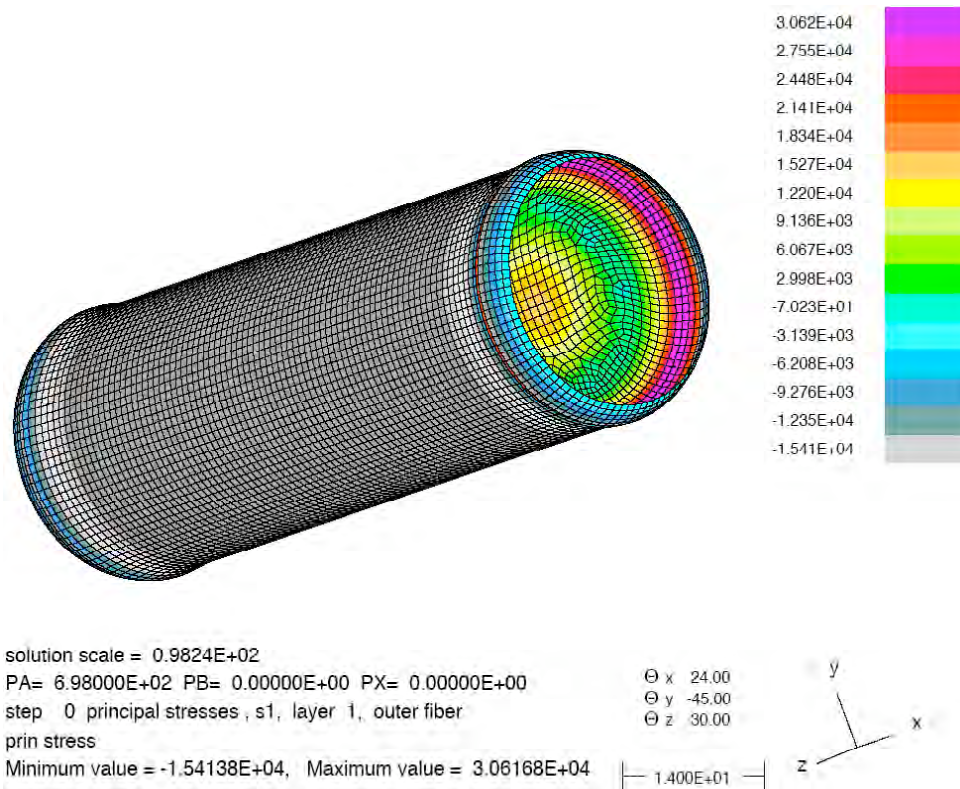


Figure B8. Principal Stress Distribution on the Exterior Surface at 679 psi.

## Critical Pressures and Depths

The stresses in the cylindrical portion of the container are compressive so yielding is not expected in this region prior to buckling. However, for the end caps, the principal stresses reach 29.6 ksi on the interior surface and 30.6 ksi on the exterior surfaces due to bending. These peak stresses are in the region (26-48 ksi) where yielding may occur. Despite the larger thickness, the end caps are more likely to yield than the cylindrical portion since they are in bending. The critical pressures and depths for each response are summarized in Table B4. Depending on material properties, the critical depth range for either end cap yielding or structural buckling to occur is between a depth of 1290 and 1520 ft. bsl.

Table B4. Critical pressures and depths from linear analysis

Cylinder Yielding	End Cap Yielding		Buckling		Critical Range	
	P <sub>cr</sub> , psi	Depth, ft. bsl	P <sub>cr</sub> , psi	Depth, ft. bsl	P <sub>cr</sub> , psi	Depth, ft. bsl
none	577-1065	1290-2390	679	1520	577-679	1290-1520

## Nonlinear Analysis with Initial Imperfections

### Buckling Analysis

An actual container will have inherent geometric irregularities and may also be dented during use, transport, or disposal. A more rigorous geometrically nonlinear analysis was performed on the container

with an initial imperfection in the cylindrical geometry. Initially, a nonlinear analysis was conducted on the container geometry without any initial imperfections, which led to inconsistent buckling pressures. Perfectly symmetrical geometries with uniform wall thicknesses and linear material properties may not analytically buckle with increasing hydrostatic pressure. In this case, the cylindrical geometry may be compressed until its radius becomes zero. However, small numerical instabilities will typically occur which will lead to the sudden collapse of the geometry but inconsistent buckling pressures. For a perfect cylinder, a linear eigenanalysis should be used to predict bifurcation-buckling load levels. Since a perfect cylinder is not practical, a nonlinear buckling analysis of the geometry containing initial imperfections will result in a more realistic prediction and, typically, lower buckling pressures.

An imperfection-sensitivity study was performed to determine the effect on the buckling pressure using the mesh with 1-inch-square elements. The internal pressure was assumed to be insensitive to container deformations. The cylinder was given an initial geometric imperfection corresponding to the buckling mode shape of the first eigenvalue ( $\phi_1$ ). An imperfection shape from an eigenvalue should provide a conservative value of the buckling pressure. The maximum amplitude of the imperfection was fixed at 1% ( $0.01t*\phi$ ), 10% ( $0.1t*\phi$ ), or 100% ( $1t*\phi$ ) of the thickness,  $t$ , of the cylindrical wall. This investigation was repeated for the mode shape corresponding to the second eigenvalue ( $\phi_2$ ). Both initial imperfections consisted of one half-wave in the longitudinal direction ( $m=1$ ). The first imperfection ( $\phi_1$ ) consisted of three full-waves in the circumferential direction ( $n=3$ ), while the second imperfection consisted of two full-waves in the circumferential direction ( $n=2$ ). These mode shapes are shown in Figures BA-1 and BA-2 in Appendix BA.

The critical pressures from these analyses are listed in Table B5 along with the eigenvalue from the linear analysis (no imperfection). For all cases, the final deformed shape is nearly identical, except for magnitude, to the shape of the initial imperfection. For initial imperfections with a magnitude of 1% of the thickness, the critical buckling pressures approached the linear eigenvalues. For magnitudes of 10% of the wall thickness, the critical buckling pressure was within 6% of the eigenvalue. For magnitudes of 100% of the wall thickness, the buckling pressure was reduced by 27% for the first imperfection shape ( $m=1, n=3$ ) and 8% for the second imperfection shape ( $m=1, n=2$ ). Overall, the buckling pressures were relatively insensitive to small imperfections in the container.

Table B5. Critical Buckling Pressures from Nonlinear Analysis

Analysis type	Imperfection amplitude ( $\alpha$ )	Initial Imperfection			
		$\Phi = \alpha\phi_1 (m=1, n=3)$		$\Phi = \alpha\phi_2 (m=1, n=2)$	
		Critical pressure, psi	Distance below sea level, ft	Critical pressure, psi	Distance below sea level, ft
Linear, Eigenvalue	0 (none)	679	1520	679	1520
Nonlinear	$t/100$	675	1510	668	1500
Nonlinear	$t/10$	640	1440	664	1490
Nonlinear	$t$	494	1110	632	1420

## Stress Analysis

As the cylindrical wall deforms due to increasing hydrostatic pressure and the presence of an initial geometrical defect, high tensile stresses develop on both the interior and exterior surfaces primarily by bending. The maximum principal tensile stresses are plotted just prior to the initiation of unstable

buckling (640 psi) for the interior and exterior surfaces in Figures B9 and B10, respectively, for the  $0.1t*\phi_1$  imperfection. The highest stresses are found in the cylindrical portion of the container and significantly exceed those in the end caps. On the interior surface, the maximum principal stress reaches 148 ksi and is centered on regions that are buckled inward. For the exterior surface, the maximum value is 132 ksi and is located in the regions that are buckled outward. Regions on the exterior surface of the cylindrical portion near the end caps also have high stresses. The maximum values exceed the yield stress and tensile strength of hot-rolled steel. Consequently, the container is expected to experience yield stresses prior to the occurrence of buckling for this case.

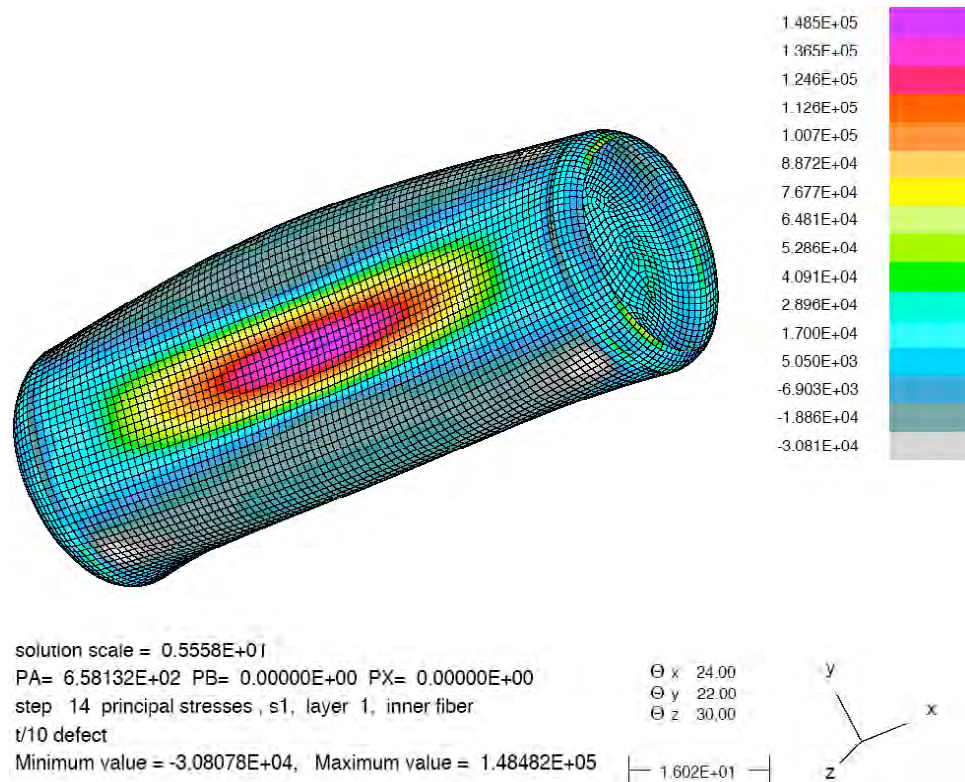


Figure B9. Maximum principal stress contours on the interior surface for  $0.1t*\phi_1$  imperfection.

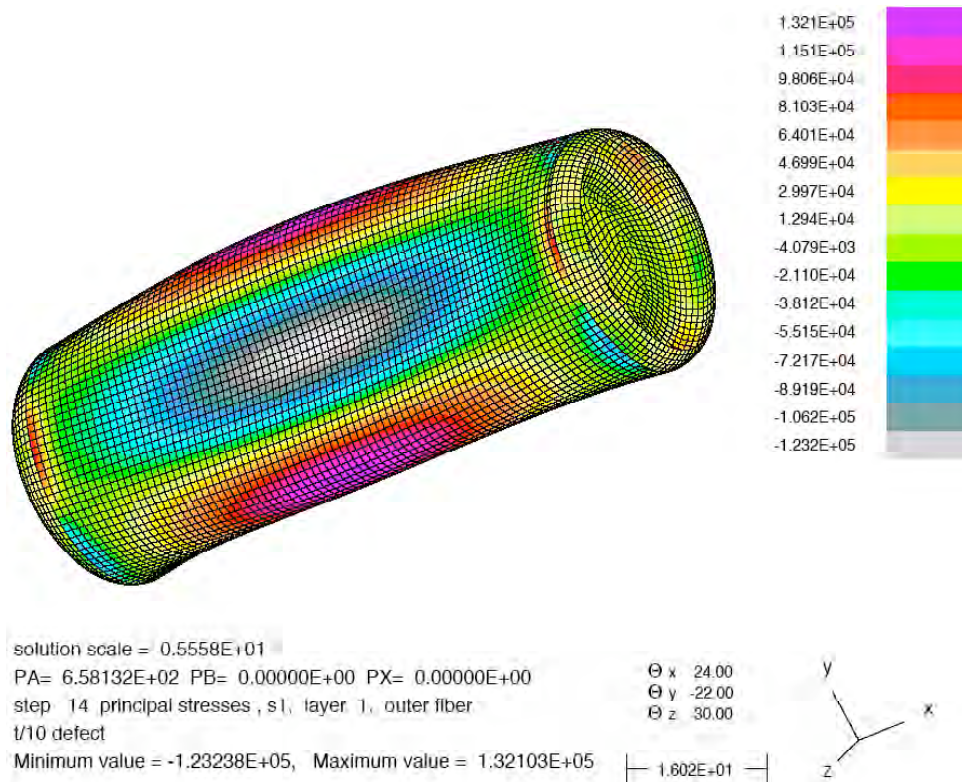


Figure B10. Maximum principal stress contours on the exterior surface for  $0.1t*\phi_1$  imperfection.

## Critical Pressures and Depths

Losses of structural integrity of the container may be caused by any one of three competing mechanisms. An example of these three mechanisms is shown as a function of equivalent external pressure for the case of a container with a  $0.1t*\phi_1$  imperfection. The maximum principal tensile stress is plotted as a function of external pressure in Figure B11 for the interior and exterior surface for both the cylindrical portion and the end caps. Initially, the principal stresses in the cylinder are compressive until non-uniform deformations develop around the initial imperfection. All the principal stresses increase nearly asymptotically as the container approaches the critical pressure where buckling occurs. For this case, the exterior surface of the end caps will yield at an external pressure of 513 to 636 psi while the interior surface will yield at a pressure of 571 to 641 psi. Similarly for the cylindrical portion, the interior and exterior surfaces will yield between 589 and 622 psi. The container is predicted to buckle at 640 psi. If the actual yield stress is below 34 ksi, the end caps are predicted to yield initially. If the actual yield stress is above 34 ksi, the cylindrical portion is expected to yield first. In either case, yielding is expected prior to the onset of buckling and should occur between 511 and 620 psi, which corresponds to depths of 1150 to 1390 ft. below sea level.

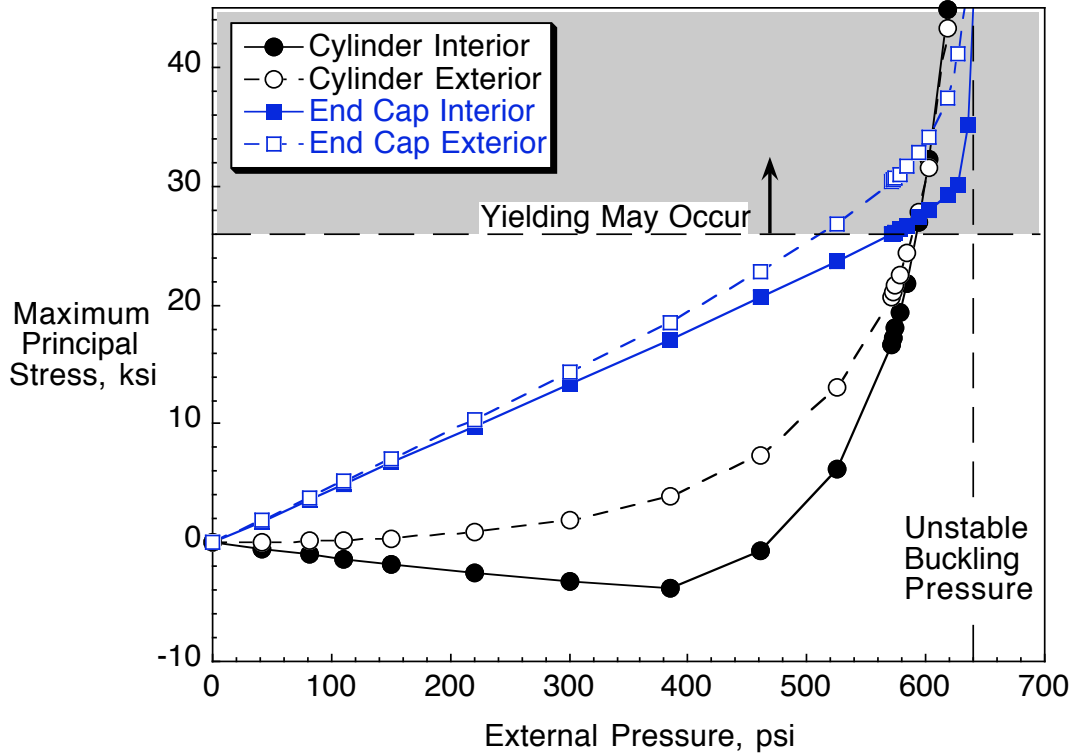


Figure B11. Maximum principal tensile surface stresses for a  $0.1t*\phi_1$  imperfection.

The critical pressures for each of the three mechanisms are summarized in Table B4 for all cases that were studied. The final columns provide an overall critical pressure and depth range. The buckling pressure generally provides an upper bound on the overall critical pressures. For all cases except the  $1t*\phi_1$  imperfection, the overall predictions did not change significantly with the imperfection shape and amplitude. However, the container with a  $1t*\phi_1$  imperfection had critical pressures that were more than 50% lower than the other conditions. A large amplitude imperfection with a deformation shape corresponding to the first eigenvalue is unlikely to occur. Excluding this case, critical depths are between 1100 to 1400 ft. below sea level.

Table B4. Critical pressures and depths for geometrically nonlinear analysis

Imperfection	Cylinder Yielding	End Cap Yielding	Buckling	Overall Prediction	
	$P_{cr}$ , psi	$P_{cr}$ , psi	$P_{cr}$ , psi	$P_{cr}$ , psi	Depth, ft. bsl
None (Linear)	-	577-1065	679	577-679	1290-1520
$0.01t*\phi_1$	-	>569	675	569-675	1280-1510
$0.1t*\phi_1$	589-622	513-636	640	513-620	1150-1390
$1t*\phi_1$	188-267	281-385	508	188-267	422-599
$0.01t*\phi_2$	-	>580	668	580-668	1300-1500
$0.1t*\phi_2$	-	>574	664	574-664	1290-1490
$1t*\phi_2$	>507	>499	632	499-632	1120-1420

## Effects of Internal Pressure

The deformations caused by the external hydrostatic pressure will cause a decrease in the internal volume with a resultant increase in the internal pressure. The increase in internal pressure may reduce the deformations relative to a given external pressure and delay the onset of buckling or yielding. The effects of the internal pressure increase will be greatest in containers with a large percentage of fluid. If the container is 100% full with an incompressible fluid, the container will never buckle or yield since the internal and external pressures will equalize. For this analysis, the fluid will be considered incompressible relative to the gas in the container. An analysis was performed to determine how an increase in internal pressure would change the results from the previous analyses. In addition, an investigation was performed to determine if there was a critical percentage of incompressible fluid, which would prevent the container from buckling or yielding.

Computer programs were written to calculate the internal volume based on nodal coordinates from the finite element model. For the cylindrical portion of the container, the volume was calculated from the coordinates of each node that makes up the cylindrical section. The total volume was the sum of 7872 individual volume calculations based on groups of four nodes. Using this technique, the calculated volume of an undeformed mesh was within 0.2% of the exact volume of a perfect cylinder. To obtain the volume from a deformed mesh, the nodal displacements were extracted from the finite element results. The original coordinates were then adjusted based on the nodal displacements. These nodal coordinates from the deformed mesh are then used as input to the computer program to calculate the volume. The volume loss is simply the volume from the deformed mesh subtracted from the initial volume. This calculation will include the volume loss due to end shortening as well as out-of-plane displacements.

The largest out-of-plane displacements were predicted to occur in the hemispherical end caps. Consequently, the volume loss due to end cap deformations also needs to be calculated. This volume loss was estimated by assuming that the deformed and undeformed shapes could be represented by the base of a sphere. This assumption is exact for the undeformed geometry since the end caps are hemispherical away from the welded region. The volume for the base of a sphere is calculated as

$$V = \frac{1}{6}\pi h(3a^2 + h^2) \quad (5)$$

where  $a$  is the radius of the base circle, and  $h$  is the height of the base of the sphere measured from the center of the base circle. The radius of the base circle,  $a$ , was fixed as the inner diameter of the cylindrical portion of the container. The change in the height of the sphere base,  $h$ , was calculated from the deformed geometry as the difference between the nodal displacement at the center of the cap and the average displacement around the circumference at the base circle (end of cylinder). The volume loss was taken as the difference between the deformed and undeformed geometries.

Initially, the reduction in volume was obtained from a linear analysis with a 679-psi external pressure (first eigenvalue). The container volume was reduced by a total of 106 in<sup>3</sup> where 77% of the loss came from deformations in the cylindrical portion and 23% was due to end cap deformations. This volume loss represents only a 0.21% reduction in the total volume. The new internal pressure,  $P_{def}$ , can be calculated using eq. 6 which is derived from the ideal gas law

$$P_{def} = \left( \frac{V_o}{V_o - \Delta V} \right) P_o \quad (6)$$

where  $P_o$  is the original internal pressure,  $V_o$  is the original volume, and  $\Delta V$  is the reduction in internal volume. Consequently, the internal pressure will only increase by 0.23% if the container is filled entirely with a gas. Similarly, the pressure will increase by 2.4%, 4.9%, and 30.3% for a cylinder containing 10%, 5%, and 1% gas, respectively. If the internal pressure is initially at atmospheric conditions, the internal pressure increases by 0.35, 0.72, and 4.45 psi for gas percentages of 10%, 5%, and 1% gas, respectively. These small increases will have a negligible influence on the external pressure for buckling since they are less than 0.7% of the critical external pressure. Consequently, these increases in internal pressure should not affect the external pressure at which initial buckling occurs.

Larger deformations with corresponding larger losses of volume are predicted using a nonlinear analysis with an initial geometric imperfection. The reduction in container volume was calculated from the nonlinear analyses for the three imperfection amplitudes corresponding to the first eigenvalue mode shape presented in the previous section. In Figure B12, the percent volume loss as a function of external pressure is shown as a curve for each imperfection amplitude. The thick dashed line represents the results from the linear analysis. For an imperfection amplitude of  $t/100$ , the volume loss as a function of pressure is nearly identical to the linear results with only a slight divergence near the critical buckling pressure. The nearly identical curves may be expected since the critical buckling pressure from the nonlinear analysis is nearly identical to the eigenvalue from the linear analysis (Table B5). For an imperfection amplitude of  $t/10$ , the volume loss curve diverges from the linear results at a much lower external pressure and increases rapidly near the critical buckling pressure. For an imperfection amplitude of  $t$ , the volume loss curve diverges immediately from the linear analysis result and continues to increase rapidly. The maximum volume losses, occurring at the critical buckling pressure, were 0.22%, 0.48%, and 6.91% for imperfection amplitudes of  $t/100$ ,  $t/10$ , and  $t$ , respectively. Consequently, significant increases in internal pressure may only occur with large imperfection amplitudes.

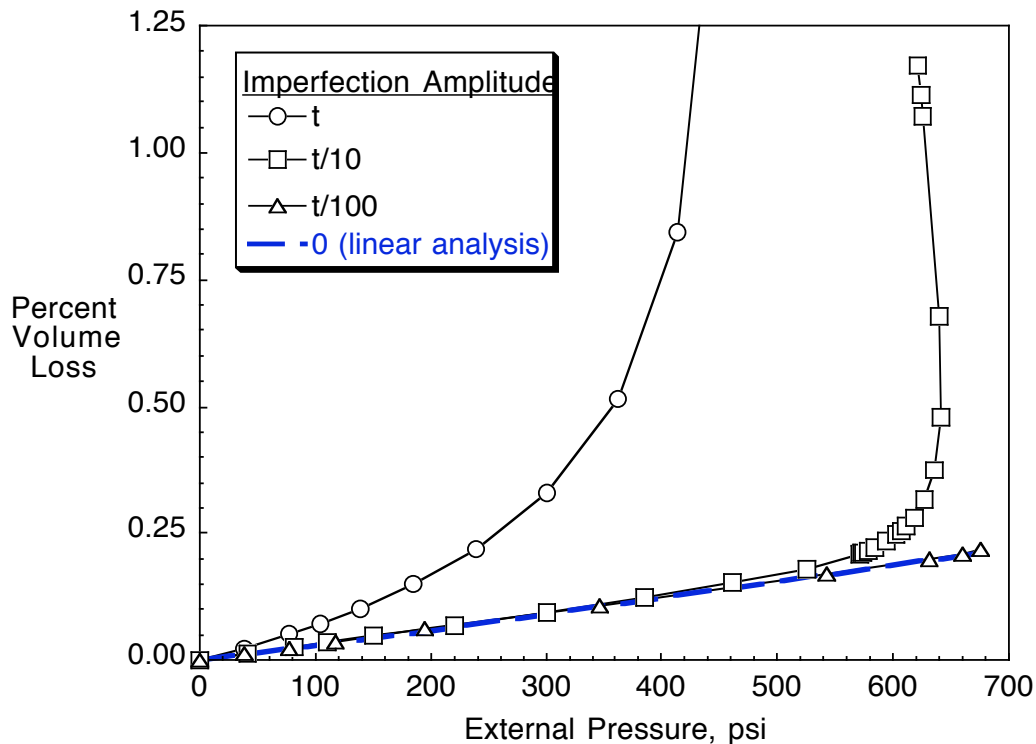


Figure B12. Volume loss curves for three imperfection amplitudes for  $\phi_1$  imperfection.

The case with the lowest critical buckling pressure and largest volume losses was for a container with an imperfection amplitude equal to the cylinder wall thickness and a buckling mode shape corresponding to the first eigenvalue. For this case, the maximum principal stresses were plotted as a function of container volume loss to determine the effect of an increase in internal pressure (Figure B13). This analysis indicates that a cylinder wall would yield at volume losses of 0.15 to 0.27%. These small reductions in overall volume would have a negligible effect on the predicted critical buckling pressure unless the cylinder contained greater than 99.5% of an incompressible fluid. Consequently, the effects of an internal pressure on the analysis can be neglected for all cases unless the container is almost entirely filled with an incompressible fluid. However, all fluids are compressible and will allow a reduction in the internal volume. However, due to plasticity of the steel material, it is possible that volume changes could become large enough to bring it into equilibrium with the external pressure.

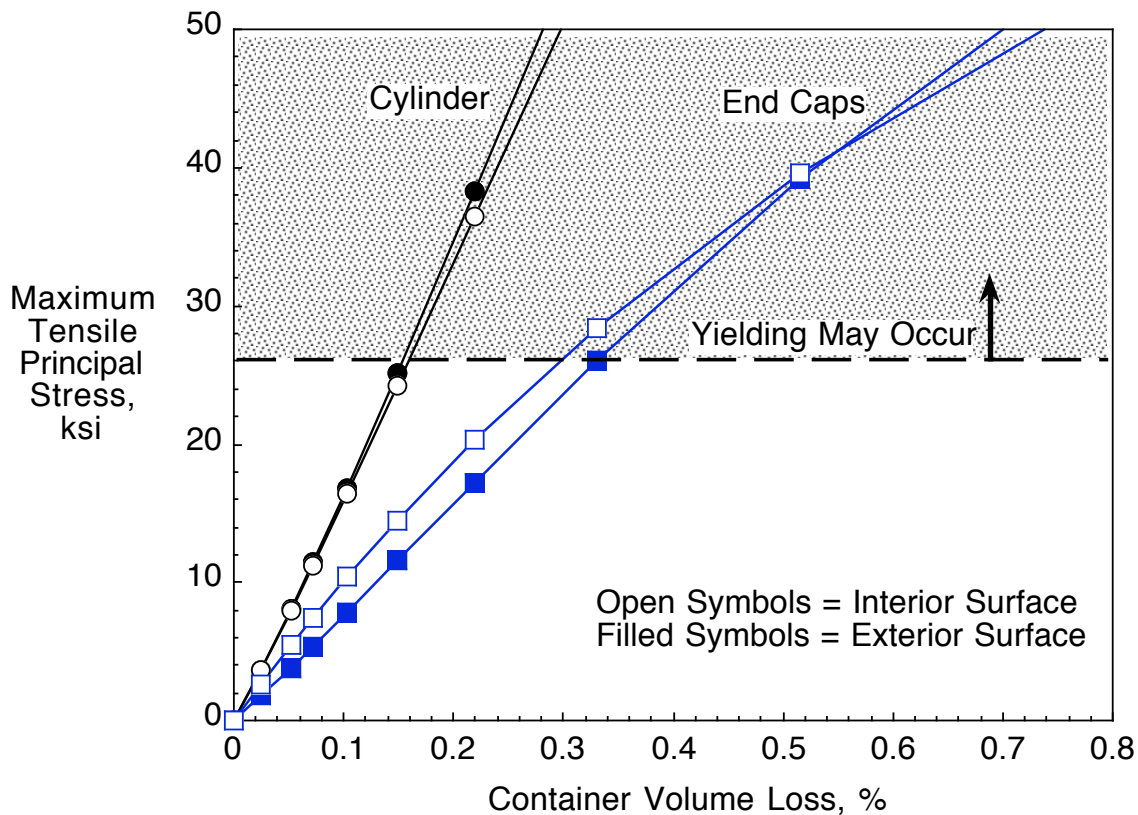


Figure B13. Maximum principal tensile stresses as a function of volume loss for  $t*\phi_1$  imperfection.

## Post-Yielding Response

The Type D container was predicted to experience localized yielding of the cylindrical wall or end caps prior to reaching unstable buckling. For both the wall and end caps, the maximum principal tensile stresses are reached as a result of bending. Consequently, the yielding will initiate on the surface. Additional information on the material properties and the internal contents is required to further analyze the response after yielding begins. Yielding has the potential to accelerate buckling or reduce the buckling pressure. However, yielding could be beneficial if the container could deform sufficiently, without failing, to reduce the pressure differential between the interior and exterior. Low-carbon steels have a maximum elongation at failure of 20 to 40%. Consequently, it is possible that the internal volume could be reduced to the volume of liquid (approximately 10% reduction) before material failure occurs.

which may limit further structural damage.

## **Additional Potential Leakage Sources**

Three potential sources of leaks that were not analyzed in this report are the forge lap welds, the vent plugs, and the valve threads. A forge lap weld is used to attach each end cap to the cylinder during manufacturing. A typical forge weld is accomplished by heating the parts, removing them from the heat source, superimposing them, and then applying pressure to the joint [5]. Forge welding was the earliest known welding process but is not routinely used today. The quality of the welded joint can vary greatly using this process. The weld may not fully take place if the two mating surfaces are not sufficiently heated. If the metal surfaces are overheated, a brittle joint of very low strength may result. The external hydrostatic pressure applied to a low quality joint may create a leakage path or cause a structural failure. The failure of the welded region was not analyzed due to a lack of specific information on joint strength and quality. Three vent plugs are installed in each end cap and are designed to rupture at 500 psi of internal pressure as a safety measure. It is unclear whether the vent plugs were replaced with solid plugs prior to sea disposal. If the vent plugs are installed, the external pressure may cause the plugs to rupture, which would provide a leakage path. Typical safety plugs will rupture with pressure applied to the opposite (non-rated) side, which would be the case for hydrostatic pressure on the container. However, the rupture pressure will likely be different from the rated relief pressure of 500 psi. If these plugs rupture due to an external pressure at 500 psi of pressure difference, the container will leak at a depth of approximately 1150 ft., assuming the internal pressure is at 14.7 psi. The valve threads may leak due to different values of thermal expansion for the end caps and the valve fittings. Leaks may also develop at the threads due to machining tolerances or due to installation problems.

## **Concluding Remarks**

The following remarks are from the investigation of a Type D one-ton container using the STAGS® structural analysis program.

1. Three basic mechanisms were investigated that may result in a loss of structural integrity: buckling initiation, cylinder yielding, and end cap yielding. Due to a lack of information, a failure of the welded region between the end caps and the cylindrical portion could not be evaluated.
2. A linear analysis of a container without imperfections showed the lowest critical buckling pressure to be 679 psi. This pressure is only 2.2% lower than the critical pressure calculated using a formula for a simple closed-end cylinder under uniform external pressure. The buckled container geometry consisted of one half wave along the length and either 2 or 3 full waves around the circumference. A stress analysis indicated that the end caps would begin yielding at external pressures between 577 and 1065 psi depending on the specific yield properties. Consequently, based on a linear analysis, critical external pressures are between 577 and 679 psi, which corresponds to a depth of 1290 to 1520 ft. below sea level.
3. Dents or other geometrical imperfections may significantly lower buckling pressures. A geometrically nonlinear analysis was performed on a container with two imperfection shapes and three imperfection amplitudes. In general, the container was found to be relatively insensitive to imperfections with low amplitudes. The worst case was for an imperfection with an amplitude of 100% of the cylinder wall thickness and a shape corresponding to the mode shape of the first eigenvalue. This imperfection reduced the buckling pressure by only 27% from the linear analysis of a defect-free container. For this case, the critical external pressures were 188 to 267 psi which corresponds to depths of 422 to 599 ft. below sea level. All other cases had significantly higher critical pressures before a loss of structural integrity.

occurred. The nonlinear analysis also showed that either the end caps or cylindrical section would likely begin yielding prior to the buckling of the container.

4. The effects of internal pressure were investigated by calculating the internal volume loss as a function of external pressure. This study showed that the container would begin yielding prior to any significant volume loss. Consequently, for buckling calculations, internal pressure increases only need to be considered when a fluid occupies more than 99% of the container volume.

5. The Type D container was predicted to yield prior to structural buckling. The yield stresses are produced on the surface primarily by localized bending. Yielding may be beneficial if the internal container volume could be reduced to near the internal fluid volume before a material failure occurs. However, additional information on the material properties and the internal contents is required to further analyze this response.

6. Three potential sources of leaks exist which were not analyzed in this report. Forge lap welds were used to attach the end caps during container manufacturing. This type of weld often has quality problems and could fail or partially fail during descent. Six vent plugs are installed in the end caps and are designed to vent at an internal pressure of 500 psi. If these are left in place and rupture due to an external pressure of 500 psi of pressure difference, the container will leak at a depth of approximately 1150 ft. The valve threads are also a potential leakage source due to thermal mismatches, machining tolerances, and installation problems.

## References

1. C.C. Rankin, F.A. Brogan, W.A. Loden, H.D. Cabiness, STAGS® User Manual — Version 5.0, Lockheed Martin Missiles and Space Co., Inc., Palo Alto, CA, Report No. LMSC P032594, 2005.
2. MSC.Patran® 2004, MSC Software Corporation, Santa Ana, CA, 2003.
3. Metals Handbook Ninth Edition, Volume 1 Properties and Selection: Irons and Steels, American Society for Metals, Metals Park, Ohio.
4. Roark's Formulas for Stress and Strain, Seventh Edition, W. C. Young and R. G. Budynas, McGraw-Hill, 2002.
5. Welding Handbook, Eighth Edition, Volume 2, R.L O'Brien, editor, American Welding Society, 1991.

## Appendix BA: Buckling Mode Shapes

The first ten eigenvalues were calculated using the mesh with 2-inch-square elements. These first ten buckling mode shapes are shown in Figures BA1-BA10. The odd-numbered modes are simple rotations of the previous mode shape.

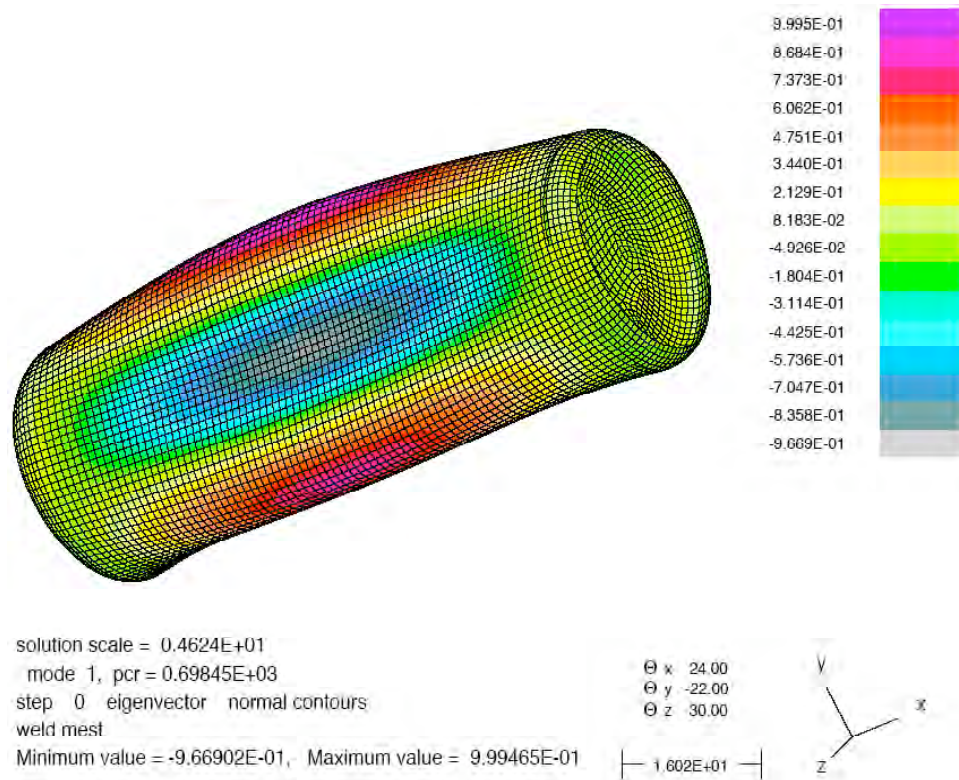


Figure BA1. Mode shape for eigenvalue 1.

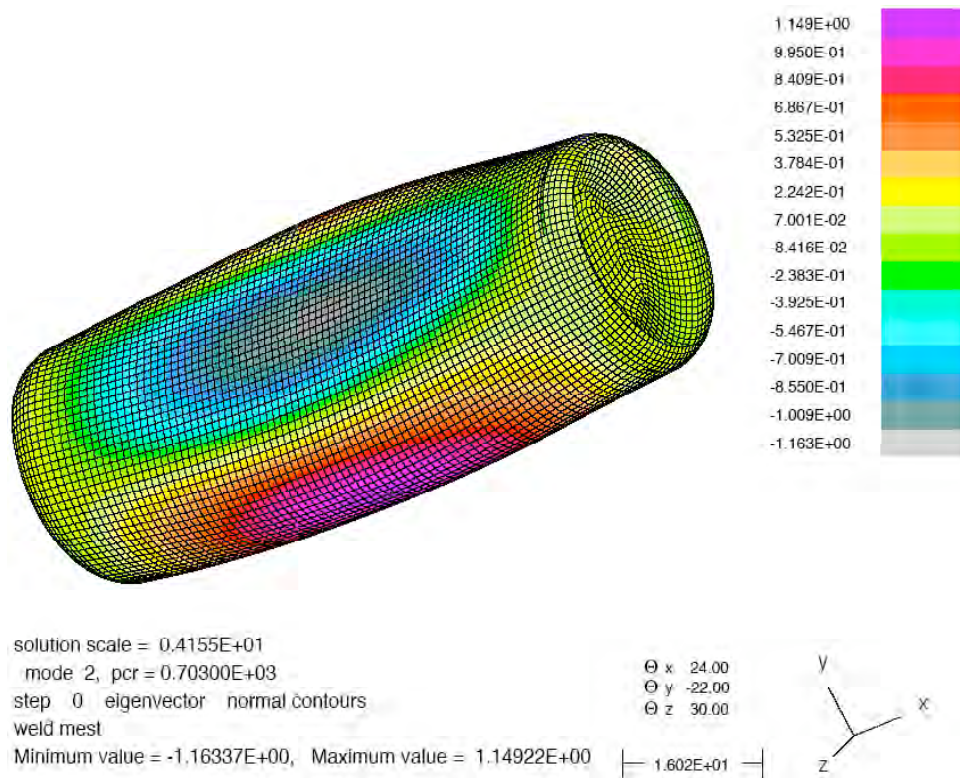


Figure BA2. Mode shape for eigenvalue 2.

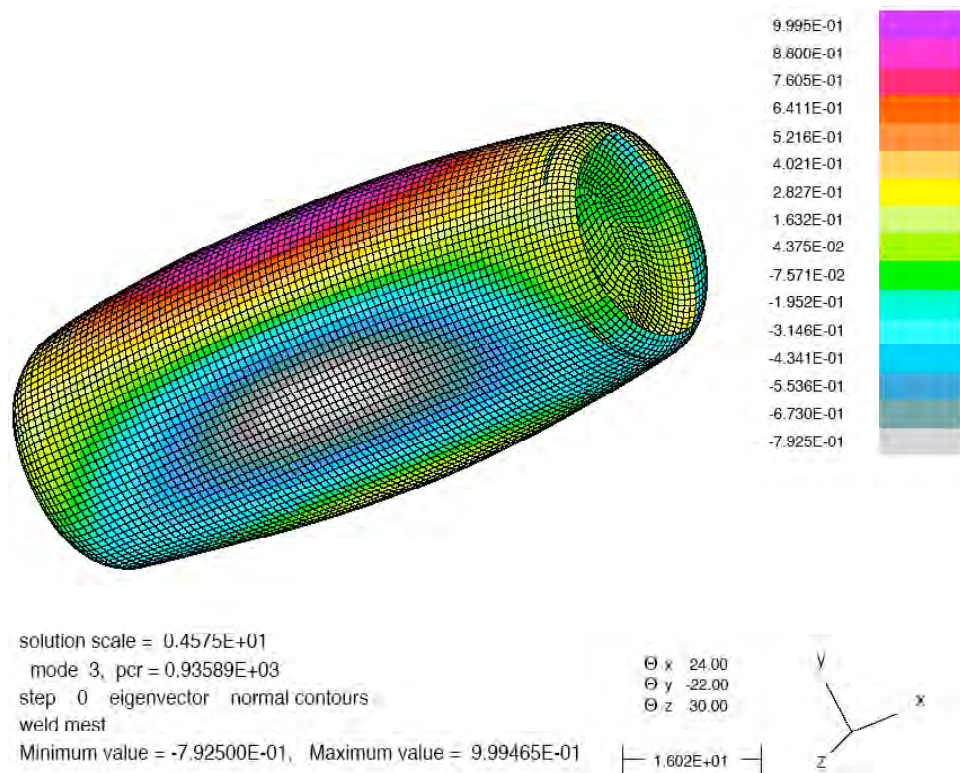


Figure BA3. Mode shape for eigenvalue 3.

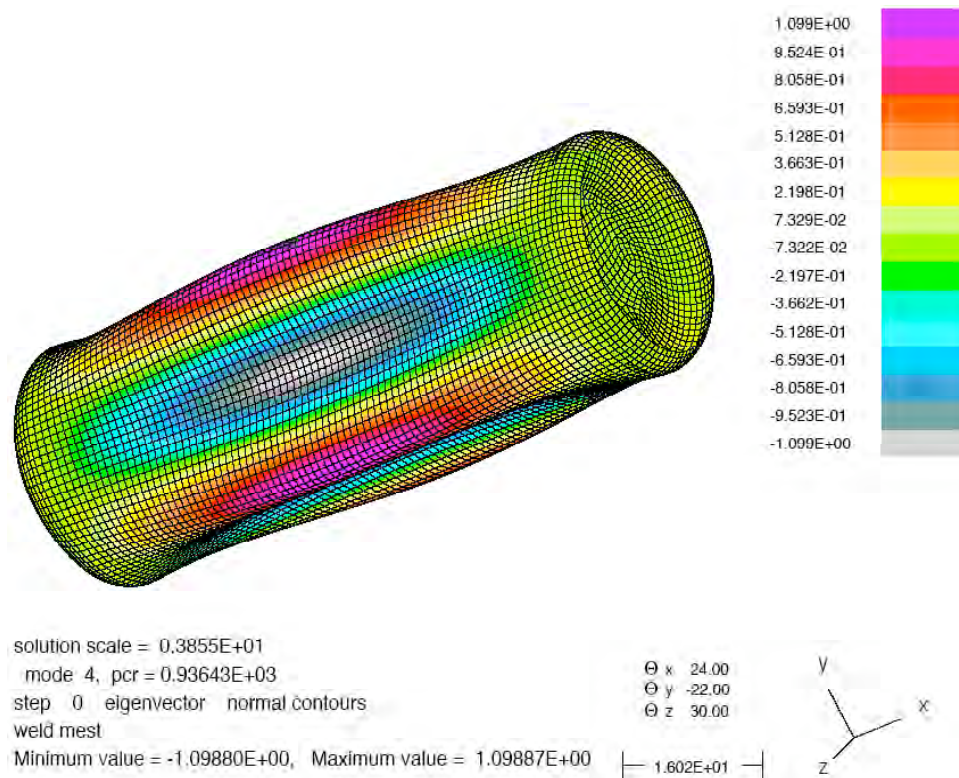


Figure BA4. Mode shape for eigenvalue 4.

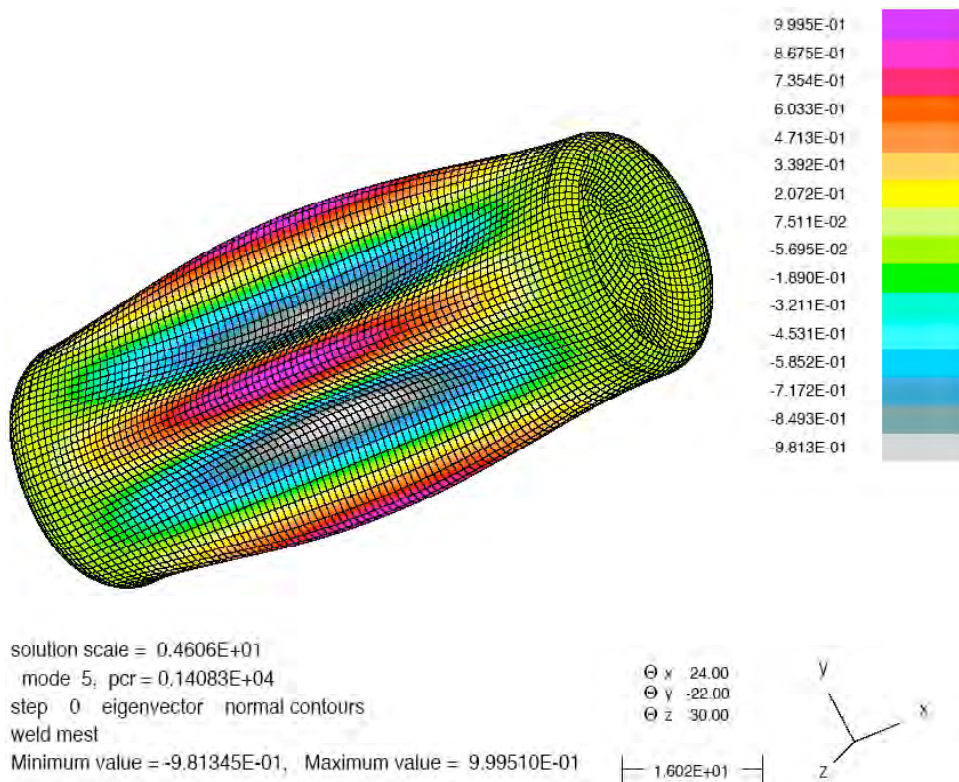


Figure BA5. Mode shape for eigenvalue 5.

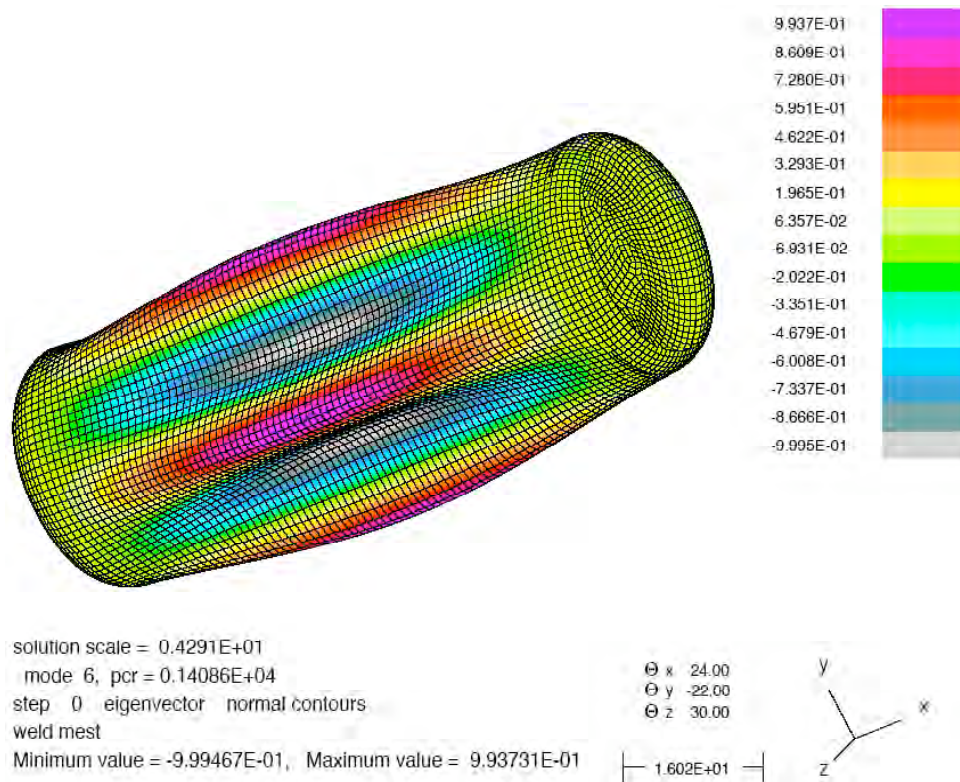


Figure BA6. Mode shape for eigenvalue 6.

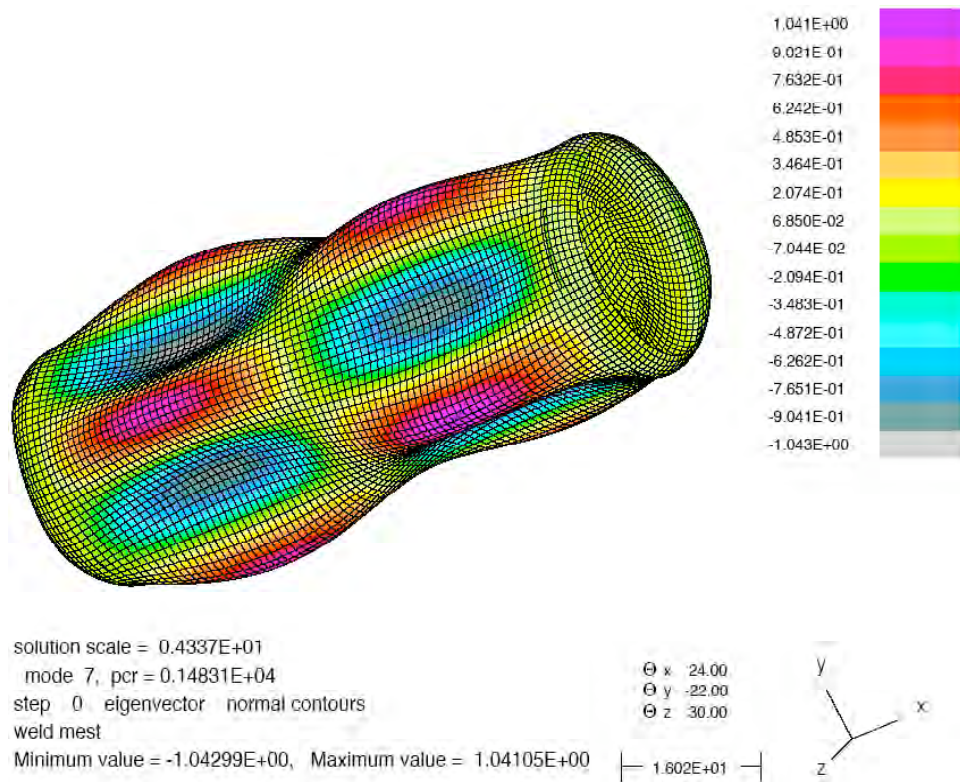


Figure BA7. Mode shape for eigenvalue 7.

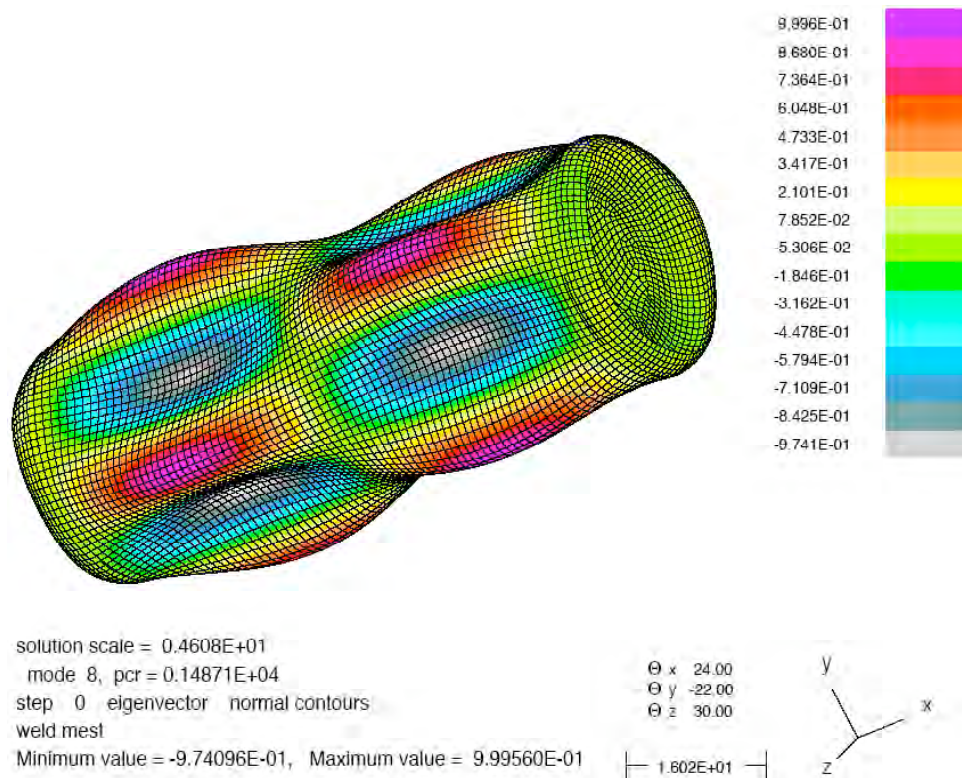


Figure BA8. Mode shape for eigenvalue 8.

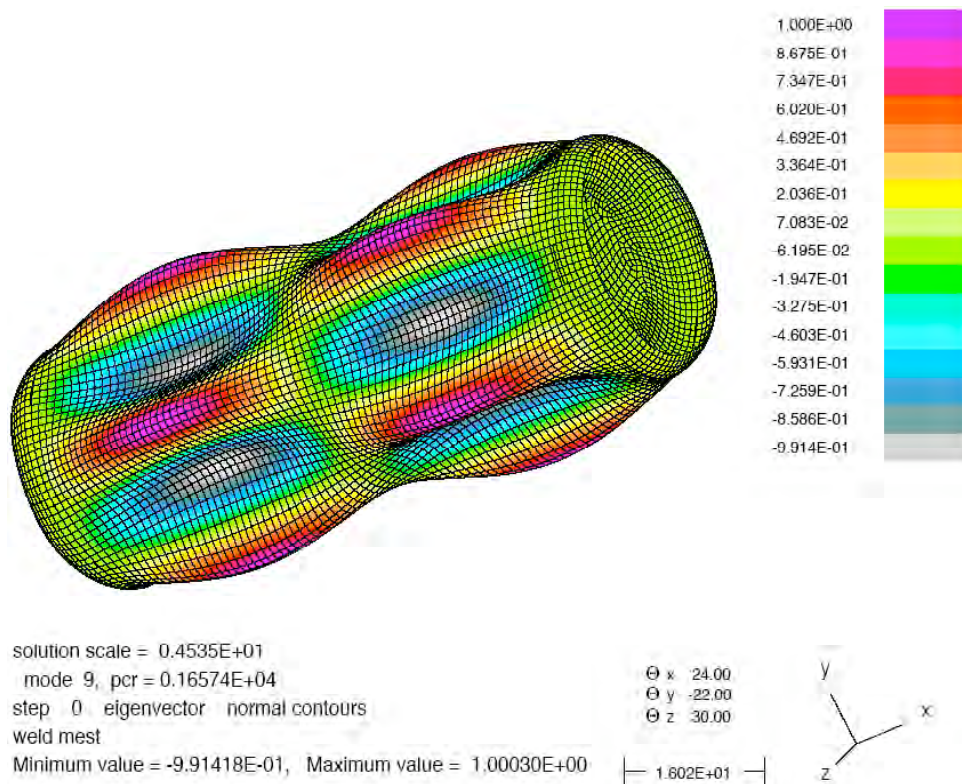


Figure BA9. Mode shape for eigenvalue 9.

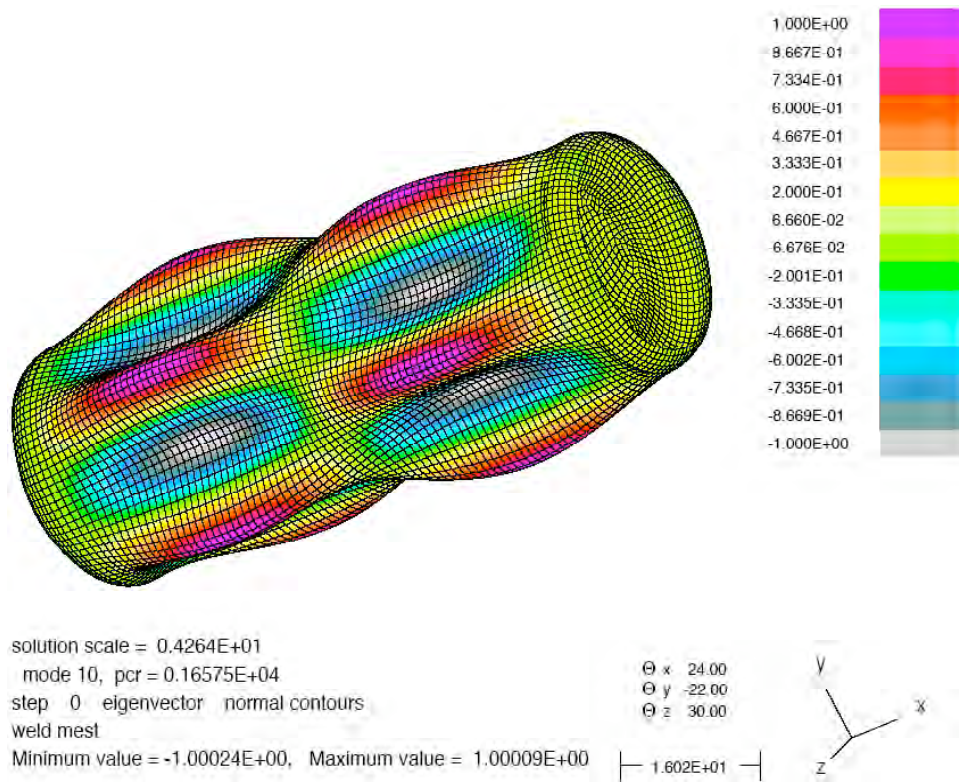


Figure BA10. Mode shape for eigenvalue 10.

# Appendix C: Simulations of a One-Ton Container Exposed to External Pressure Using an Explicit, Transient Dynamic, Finite Element Code (LS-DYNA<sup>®</sup>)

Karen E. Jackson and Edwin L. Fasanella  
NASA Langley Research Center  
Hampton, VA

## Introduction

An explicit, transient dynamic finite element code, LS-DYNA<sup>®</sup> [1], was used to simulate the structural response of a Type D one-ton chemical container loaded by an external pressure representing disposal at sea. The one-ton containers are fabricated of hot-rolled steel with dimensions of 81.5-in. in length and 30-in. in diameter. The Type D container is cylindrical in shape with two concave hemispherical end caps. The cylinder wall has a thickness of 0.41-in., and the end caps are 0.75-in. thick. The containers were reported to be 90% full. An assembly drawing of the container is shown in Figure 1 of the main section of this report. The objective of the simulation was to address the structural response of a pristine one-ton container during sea disposal due to the effects of hydrostatic pressure. A maximum disposal depth of 17,000 ft. (3.22 miles) was assumed.

LS-DYNA<sup>®</sup> [1], marketed by Livermore Software Technology Corporation (LSTC), was used to simulate the structural response of a one-ton cylindrical container with concave hemispherical end caps. The LS-DYNA<sup>®</sup> model was executed without the internal contents to determine the buckling load of the container. Data from these simulations were compared with the results from the STAGS<sup>®</sup> linear buckling analyses (Appendix B). There are significant differences in the two codes. For example, STAGS<sup>®</sup> is a structural analysis code in which global stiffness matrices are formed, and an eigenvalue problem is solved to determine when buckling will occur. LS-DYNA<sup>®</sup>, however, is a transient dynamic finite element code that solves equations of motion using an explicit time integration approach, and for this case buckling will be indicated when the shape changes rapidly.

Analytical techniques were also developed to simulate the effects of the internal contents on the structural response and the subsequent impact with the ocean floor. As the container's internal volume decreases due to the external pressure, the internal pressure will increase resulting in a reduced pressure differential between the interior and exterior. Consequently, the critical external pressure or critical depth where significant structural damage occurs may increase. To achieve a significant increase in the internal pressure, the interior volume must be reduced to near the volume of the fluid contents. The container will have to undergo yielding to obtain this amount of volume reduction. Therefore, this analysis is highly dependent on specific material response properties up to failure in both tension and compression. Since these properties were not available, no results of this investigation will be presented. In the following sections of the paper, the model development and the analytical results for the empty container are presented. Brief descriptions of the models to simulate the internal contents and the impact with the ocean floor are also given.

## Container Model

A simplified geometry model of the container was created in MSC.Patran® [2], a pre- and post-processing software package marketed by MSC.Software, Inc. The geometry was meshed, element properties were assigned, and an LS-DYNA® input model was generated. The LS-DYNA® model of the container, shown in Figures C1 and C2, contained three separate parts: the cylinder wall, end caps, and end cap sleeves. This model contained: 9,752 Belytschko-Tsay shell elements and 79,050 nodes. The nominal element edge length of the mesh is 1 inch.

A \*MAT\_PLASTIC\_KINEMATIC material property was used to represent the steel properties of the container. This material definition in LS-DYNA® allows for a linear elastic response up to a specified yield stress, followed by a plastic response to ultimate failure. The LS-DYNA® simulations were executed using the same material properties as used for the buckling analysis in Appendix B. The specific properties, listed in Table B1, are for AISI 1020 hot-rolled steel. For the LS-DYNA® simulations, a lower-bound yield stress of 26,000 psi was used. Note that modeling of the fluid contents will be discussed in a later section of the paper.

A linearly increasing external hydrostatic pressure was applied to elements in the model using the \*LOAD\_SHELL\_SET command in LS-DYNA®. Initially, a maximum pressure loading of 7,573 psi was used. This value was calculated based on the estimated hydrostatic pressure at a depth of 17,000 ft. The pressure was applied to the elements forming the cylinder wall and the end caps, but not to the end cap sleeves since both sides of the sleeves are exposed to the hydrostatic pressure.

In the model, the end caps and end cap sleeves together weighed 491 lbm and the cylinder wall weighed 798 lbm. Thus, the total weight of the container without contents is 1,289 lbm. In comparison, the actual container is reported to weigh 1,600 lbm. The origin of the model and the center-of-gravity are located at  $x = 0$  in.,  $y = 0$  in., and  $z = 0$  in., which represents the center point of the mid-plane of the model. The x-axis is oriented along the longitudinal axis of the cylinder, as shown in Figure C1. The y-axis is normal to the x-axis and points vertically upwards, while the z-axis points to the right. Thus, a right-handed coordinate system was used.

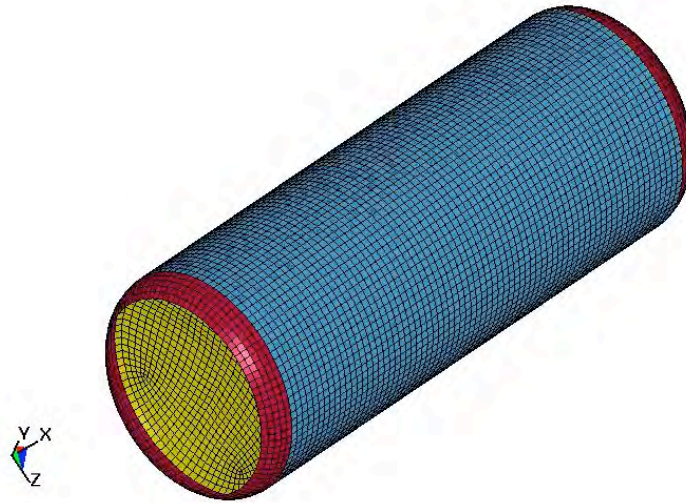
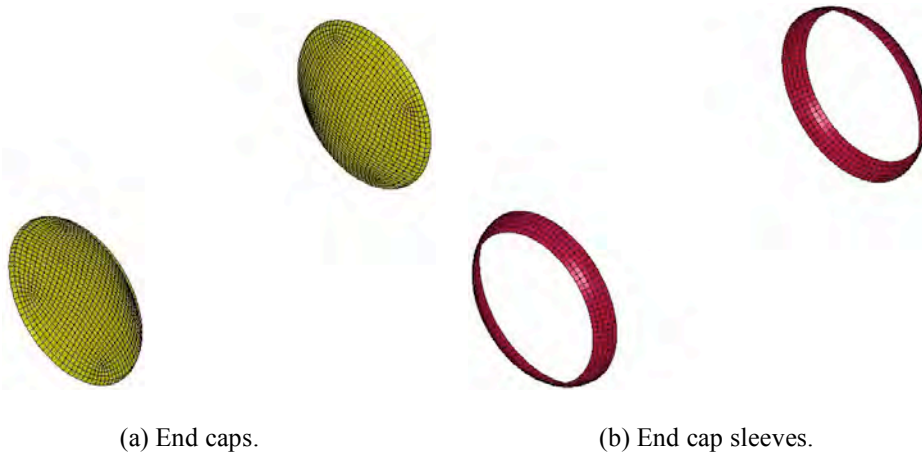
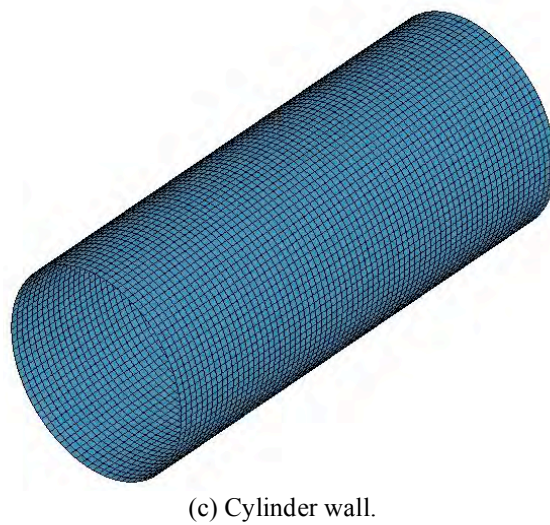


Figure C1. LS-DYNA® model of the container.



(a) End caps.

(b) End cap sleeves.



(c) Cylinder wall.

Figure C2. LS-DYNA® model parts.

## **Simulations of Internal Contents and Impact**

LS-DYNA® models were developed to simulate the 90%-filled container when subjected to external hydrostatic pressure and impact with the ocean floor. Two approaches were used to simulate the internal contents. In the first approach, the interior space within the container was completely meshed with solid elements. The solid elements were assigned a material property that was based on the ideal gas law and input into the LS-DYNA® model using a \*DEFINE\_CURVE option. This material model was used to simulate a 10% gaseous volume combined with a 90% fluid volume. For the initial simulation, the fluid was assumed to be water. Near 10% volumetric strain, a dramatic increase in internal pressure occurs up to the pressure to be in equilibrium with the external pressure. After a volumetric strain of approximately 10% is achieved, a linear curve with a slope of 300,000 psi (the approximate bulk modulus of water) is input. For example, at a depth of 17,000 ft, water exhibits a volumetric strain of approximately 2%. Thus, at a maximum disposal depth of 17,000 ft., the container with 10% gas (or air) would experience a volumetric strain of about 12%. With accurate material failure properties, this analysis would be expected to give reasonable predictions of container rupture due to hydrostatic external pressure.

A second approach to represent the fluid contents would be to perform a coupled fluid-structure interaction simulation using the Arbitrary Lagrange Euler (ALE) formulation within LS-DYNA®. For this type of simulation, a fixed grid of solid elements is created to fill the interior of the container. The liquid and gaseous portions of the contents would be represented using the appropriate Equations of State (EOS). A coupling surface would be defined between the fluid contents and the elements forming the container model. As external hydrostatic pressure is applied, the container deforms and the fluid contents react to the applied pressure loading. Note that for ALE simulations, the element grid remains fixed in space; however, the fluid contents are free to move from element to element in the interior of the container in response to the applied load. The ALE approach is the most accurate method of modeling fluid/liquid/gaseous contents within the container. However, precise information would be needed to define the EOS. Also, material failure data for the container would have to be provided in order to predict rupture.

The model filled with solid elements was also used to simulate the impact with the ocean floor. This model combined the loading of the externally applied hydrostatic pressure with the impulsive loading simulating the impact with the ocean floor. The value of terminal velocity, 13.2 ft/s, was specified as a requirement for the impact simulation. It is interesting to note that a container falling at a constant velocity of 13.2 ft/s would require 21.5 minutes to reach a depth of 17,000 ft. The model is translating vertically downward in the negative y-direction and impacts at an attitude where the x-direction is parallel to the ocean floor. An impact velocity was assigned to all of the nodes in the container model, and a soil model was added to represent the ocean floor. The soil model is representative of a soft soil found at the Utah Test and Testing Range (UTTR) and was developed at NASA Langley for test-analysis correlation studies related to the Mars Sample Return (MSR) program [3]. A contact definition was used to represent the container impact with the ocean floor. Without material property data that accurately represents the complete failure response of the steel in the container, rupture of the container cannot be predicted.

## **Analytical Predictions – No Internal Contents**

LS-DYNA® simulations were executed in which an external hydrostatic pressure, linearly increasing from 0 to 7,573-psi, was applied to the elements forming the end caps and the cylinder wall of the model. The external pressure was reduced from the original value of 7,573 psi to 800 psi based on initial

LS-DYNA® simulations, which showed that buckling of the container occurred at a much lower value of external pressure. No internal contents were included in this model. The termination of the LS-DYNA® dynamic simulation was selected to provide a converged response. LS-DYNA® simulation results and comparisons with the STAGS® [4] results are presented.

Contour plots of resultant displacement are shown in Figure C3 for increasing external pressures in the model approaching the buckling pressure and just after buckling. Each contour plot has a different fringe level. The magnitudes of the fringe levels change dramatically for external pressures between 699 and 701 psi, increasing from a maximum of 0.53 in. at 699 psi to 5.7 in. at 701 psi. These results indicate that buckling occurs between 699 and 701 psi.

To further clarify the precise external pressure at initial buckling, a plot of diameter versus external pressure is shown in Figure C4. The diameter is nearly constant at 30 in. until dramatic changes in diameter occur just before 700 psi. From this plot, it is evident that buckling occurs at 699.2 psi, which is rounded to 699 psi. The diameter was established as the length between two opposing cylinder nodes near the mid-plane of the container.

A fringe plot of in-plane longitudinal stress is shown in Figure C5. This fringe plot was obtained for an external pressure of 699 psi. The fringe ranges for the plot shown in Figure C5 have been set to match those of the plot of axial stress from the STAGS® linear buckling analysis, shown in Figure B6. The plot of axial stress from the STAGS® model was obtained for an external pressure of 679 psi, which is the buckling pressure obtained from the linear structural analysis. These two plots are very similar. In both plots the longitudinal stress in the cylinder is compressive and is nearly constant through the cylinder. Also, stress variations are seen near the interface between the cylinder and the end cap sleeves. The concave surface of the end cap exhibits the highest tensile stress. Note that no comparison with the hoop stress was possible since the LS-DYNA® simulations were not performed using cylindrical coordinates.

These results indicate that the linear buckling and explicit dynamic simulations are providing comparable initial buckling pressures, such that the LS-DYNA® buckling pressure (699 psi) is only 3% higher than the STAGS® buckling pressure (679 psi). In fact, the buckling pressure for the dynamic solution is expected to be slightly higher than the buckling pressure obtained from the linear, structural buckling simulation since the LS-DYNA® analysis incorporates some minimal inertial effects. There are no inertial effects in the static STAGS® simulation.

One concern in applying an explicit, transient dynamic code to simulate an essentially quasi-static problem, such as the initial buckling behavior of the empty container, is to ensure that the kinetic energy of the simulation is very low in comparison to the internal and/or strain energy. Therefore, the internal and kinetic energy time histories were output from the simulation and are plotted in Figure C6. The results shown in Figure C6 indicate that the kinetic energy is essentially zero until buckling occurs. Conversely, the internal energy increases gradually with increasing external pressure, until buckling occurs. At 700-psi, both curves increase rapidly as buckling and collapse of the structure occurs.

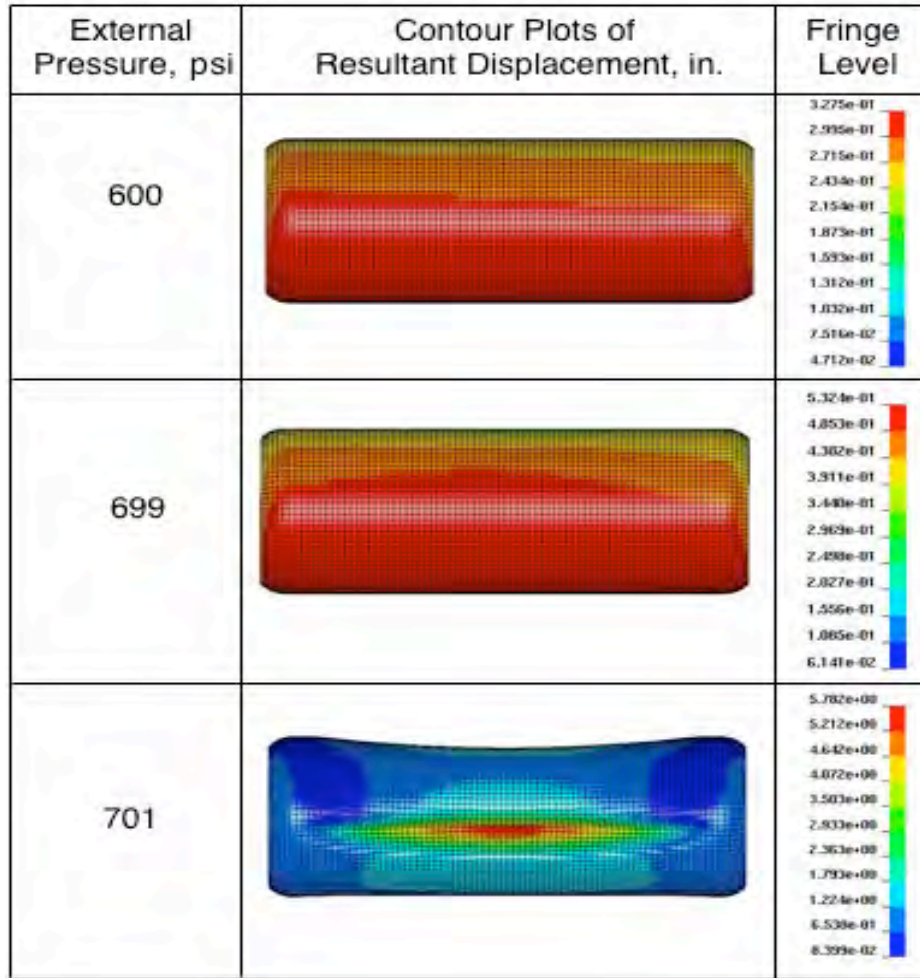


Figure C3. Contour plots of resultant displacement for the model without internal contents.

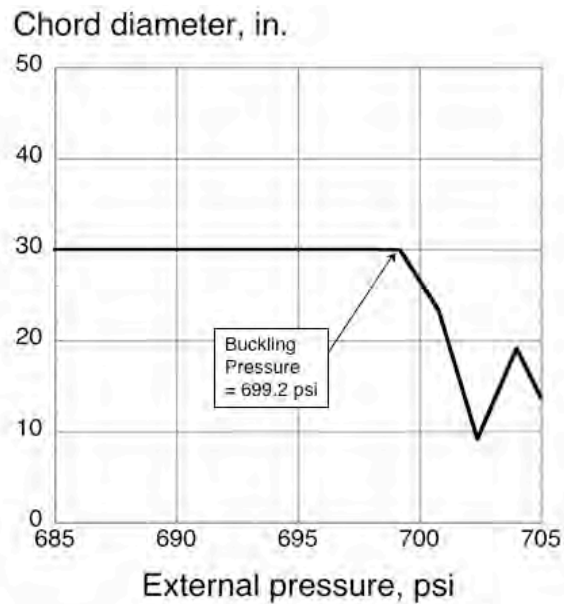


Figure C4. Plot of mid-plane diameter versus external pressure.

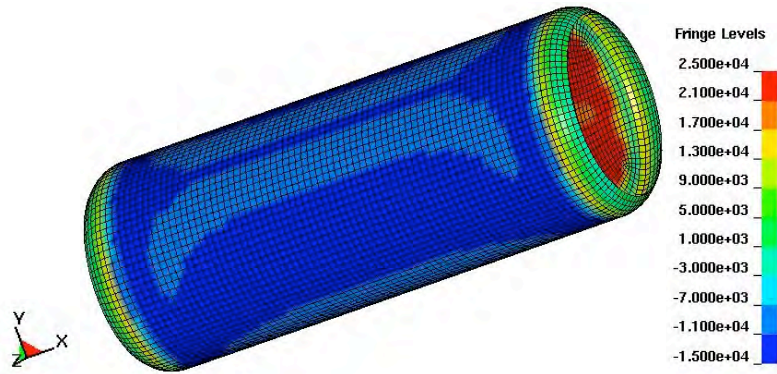


Figure C5. Fringe plot of in-plane stress at 699-psi external pressure.

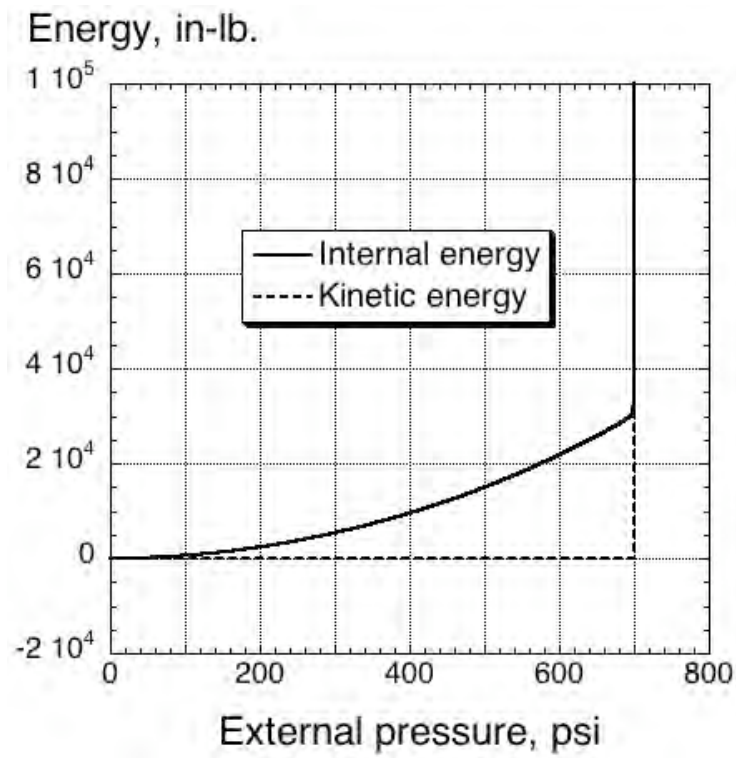


Figure C6. Comparisons of internal versus kinetic energy for the LS-DYNA® simulation.

## Concluding Remarks

An analytical study was conducted to determine the survivability of a cylindrical container with concave hemispherical end caps during sea disposal. An LS-DYNA<sup>®</sup> finite element model of the container was developed based on an assembly drawing. Material properties representative of AISI 1020 steel were selected for the cylinder wall, end caps, and end cap sleeves.

The LS-DYNA<sup>®</sup> model was executed without internal contents to determine the buckling load of the container for the case of externally applied loads only. Linearly increasing external hydrostatic pressure up to 800 psi was applied to the container to determine the initial buckling. The LS-DYNA<sup>®</sup> simulation predicted that initial buckling would occur for an external pressure of 699.2 psi. This value is only 3% higher than the buckling pressure predicted by the STAGS<sup>®</sup> simulation (679 psi) described in Appendix B. The consistency of the results provides confidence in the container model for use in additional simulations.

Finally, two approaches were discussed to represent the fluid contents within the container. In order to predict rupture of the tank, accurate material failure data must be supplied. Additional details on the valves, threads, welds, etc. are required to further determine the survivability during sea disposal. This information was not provided, thus, the LS-DYNA<sup>®</sup> simulations of sea disposal and the sea floor impact are not included.

## References

1. Anon., "LS-DYNA<sup>®</sup> Keyword User's Manual – Version 970," Livermore Software Technology Company, Livermore, CA, April 2003.
2. Anon., "MSC.Patran<sup>®</sup>," Publication No. 903077, Version 6, The MacNeal-Schwendler Corporation, 1996.
3. Fasanella, E. L., Jones, Y. T., Kellas, S., and Knight, N. F., Jr., "Earth Impact Studies for Mars Sample Return," AIAA Journal of Spacecraft and Rockets, Vol. 39, No. 2, March-April 2002, pp. 237-243.
4. C.C. Rankin, F.A. Brogan, W.A. Loden, H.D. Cabiness, STAGS<sup>®</sup> User Manual — Version 5.0, Lockheed Martin Missiles and Space Co., Inc., Palo Alto, CA, Report No. LMSC P032594, 2005.

REPORT DOCUMENTATION PAGE					Form Approved OMB No. 0704-0188	
<p>The public reporting burden for this collection of information is estimated to average 1 hour per response, including the time for reviewing instructions, searching existing data sources, gathering and maintaining the data needed, and completing and reviewing the collection of information. Send comments regarding this burden estimate or any other aspect of this collection of information, including suggestions for reducing this burden, to Department of Defense, Washington Headquarters Services, Directorate for Information Operations and Reports (0704-0188), 1215 Jefferson Davis Highway, Suite 1204, Arlington, VA 22202-4302. Respondents should be aware that notwithstanding any other provision of law, no person shall be subject to any penalty for failing to comply with a collection of information if it does not display a currently valid OMB control number.</p> <p><b>PLEASE DO NOT RETURN YOUR FORM TO THE ABOVE ADDRESS.</b></p>						
1. REPORT DATE (DD-MM-YYYY)		2. REPORT TYPE		3. DATES COVERED (From - To)		
01-07 - 2007		Technical Memorandum				
4. TITLE AND SUBTITLE Analysis of the Effects of Sea Disposal on a One-Ton Container				5a. CONTRACT NUMBER		
				5b. GRANT NUMBER		
				5c. PROGRAM ELEMENT NUMBER		
6. AUTHOR(S) Jackson, Wade C.; Jackson, Karen E.; Fasanella, Edwin L.; and Kelley, John				5d. PROJECT NUMBER		
				5e. TASK NUMBER		
				5f. WORK UNIT NUMBER 732759.07.09		
7. PERFORMING ORGANIZATION NAME(S) AND ADDRESS(ES) NASA Langley Research Center      U.S. Army Research Laboratory Hampton, VA 23681-2199      Vehicle Technology Directorate NASA Langley Research Center Hampton, VA 23681-2199				8. PERFORMING ORGANIZATION REPORT NUMBER  L-19368		
9. SPONSORING/MONITORING AGENCY NAME(S) AND ADDRESS(ES) National Aeronautics and Space Administration Washington, DC 20546-0001 U.S. Army Research Laboratory Adelphia, MD 20783				10. SPONSOR/MONITOR'S ACRONYM(S)  NASA		
				11. SPONSOR/MONITOR'S REPORT NUMBER(S) NASA/TM-2007-214881    ARL-TR-3883		
12. DISTRIBUTION/AVAILABILITY STATEMENT Unclassified - Unlimited Subject Category 39 Availability: NASA CASI (301) 621-0390						
13. SUPPLEMENTARY NOTES An electronic version can be found at <a href="http://ntrs.nasa.gov">http://ntrs.nasa.gov</a>						
14. ABSTRACT Excess and obsolete stocks of chemical warfare material (CWM) were sea disposed by the United States between 1919 and 1970. One-ton containers were used for bulk storage of CWM and were the largest containers sea disposed. Disposal depths ranged from 300 to 17,000 feet. Based on a Type D container assembly drawing, three independent analyses (one corrosion and two structural) were performed on the containers to address the corrosion resistance from prolonged exposure to sea water and the structural response during the descent. Corrosion predictions were made using information about corrosion rates and the disposal environment. The structural analyses employed two different finite element codes and were used to predict the buckling and material response of the container during sea disposal. The results of these investigations are summarized below. Detailed reports on each study are contained in the appendices.						
15. SUBJECT TERMS Container; Buckling; Corrosion; Hydrostatic pressure; Sea disposal						
16. SECURITY CLASSIFICATION OF:			17. LIMITATION OF ABSTRACT	18. NUMBER OF PAGES	19a. NAME OF RESPONSIBLE PERSON	
a. REPORT	b. ABSTRACT	c. THIS PAGE			STI Help Desk (email: <a href="mailto:help@sti.nasa.gov">help@sti.nasa.gov</a> )	
U	U	U	UU	50	19b. TELEPHONE NUMBER (Include area code) (301) 621-0390	